# Lecture Notes on Statistical Physics and Spin Glasses

Haijun Zhou

Institute of Theoretical Physics,
the Chinese Academy of Sciences,
Zhong-Guan-Cun-Dong-Lu 55, Beijing 100080, China
Email: zhouhj@itp.ac.cn



April 28, 2006

# Preface

This is the lecture notes for an *Advanced Graduate Course on Statistical Physics and Spin Glasses* given by the author at ITP in the period of 21 Nov 2006 – 09 Jan 2006. This graduate course was aimed for students who have some knowledge about statistical mechanics and who are interested in spin glasses but without any background.

In these lecture notes, I do not attempt to be complete. Many important topics are not mentioned. For each topic that is mentioned in these notes, the basic concepts are introduced by working on some specific models.

I thank Dr. Yaogen Shu and Dr. Jianjun Zhou for their valuable helps in typing out some parts of these notes.

# Contents

# Chapter 1

# Some Basic Concepts of Statistical Physics

**Classical Mechanics:** macroscopic objects; few-body systems; energy scale $\gg$ thermal energy $k_BT$.

**Quantum Mechanics:** microscopic objects ($\sim 10^{-10}$m or even smaller); few-body systems; energy scale $\gg$ thermal energy (usually).

**Statistical Mechanics:** many-body systems; internal interactions. It aims at understanding the macroscopic properties of a given many-body system in terms of microscopic interactions.

For the benefit of later discussion, here we introduce some basic concepts of equilibrium statistical physics. The reader is referred to textbooks (e.g., [1, 2]) for more rigorous definitions of these concepts.

## 1.1 Subsystem

A subsystem in a statistical physical system is a part of an isolated system (say, the whole universe). It also contains a huge number of particles. The subsystem can exchange energy or even particles with its surrounding environment (see Fig. 1.1).

Denote the energy of subsystem as $E$ and its number of particles as $N$. Since the subsystem is open, its energy $\mathcal{E}$ is not a constant; it will fluctuate

arround certain averaged value $\langle \mathcal{E} \rangle$ with time. However, when the system size $\mathcal{N}$ is sufficiently large, it is usually the case that

$$\langle \mathcal{E} \rangle \propto \mathcal{N} \ , \tag{1.1}$$

while the standard deviation of the energy fluctuation is

$$\sigma_{\mathcal{E}} \equiv \sqrt{\langle \mathcal{E}^2 \rangle - \langle \mathcal{E} \rangle^2} \propto \mathcal{N}^{1/2} \ . \tag{1.2}$$

In typical cases, the number of particles in a system is at least of the order $\mathcal{N} \sim 10^{23}$. In such cases, $\sigma_{\mathcal{E}}/\mathcal{E} \propto \mathcal{N}^{-1/2} \to 0$. In other words, the total energy (or more precisely, the energy density) of the subsystem can be regarded as constant.

The microscopic state of the system is, of cause, not fixed. It will change with time and form a very complicated trajectory in the phase space of the subsystem.

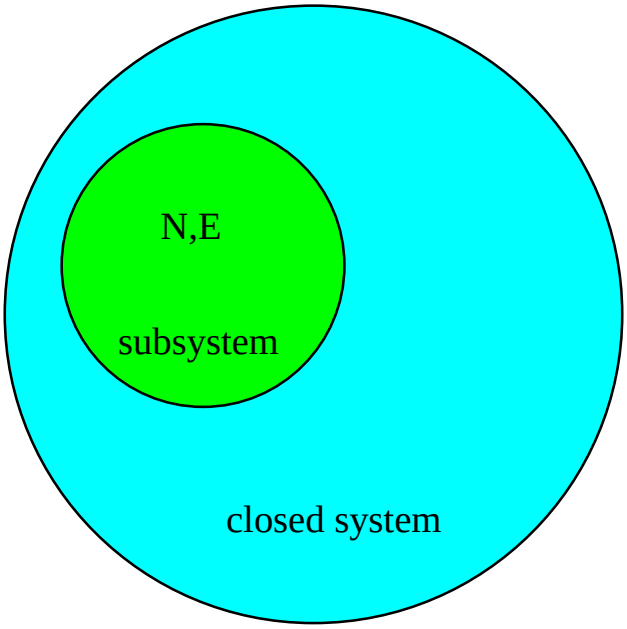


Figure 1.1: A macroscopic subsystem that is part of an isolated (closed) system. The subsystem can exchange energy (and matter) with the remaining part of the closed system.

## 1.2 Ergodicity

Consider a subsystem whose number of particles is fixed. Denote the total number of possible microscopic configurations of a subsystem as $\Omega$. Some of these configurations have energy that are markably deviated from the mean energy $\langle \mathcal{E} \rangle$ of the subsystem. As we know from the preceding section that, these microscopic configurations has *no* contribution to the statistical physical property of the subsystem. Only those microscopic configurations with energy density equaling to the subsystem's mean energy density will contribute to the subsystem's macroscopic property. Denote the total number of such configurations as $\Omega(\langle \mathcal{E} \rangle)$. Usually, $\Omega(\langle \mathcal{E} \rangle) \ll \Omega$.

The ergodicity concept means that, starting from any given intial configuration of the subsystem, the subsystem will be able to arrive at each of those $\Omega(\langle \mathcal{E} \rangle)$ microscopic configurations sooner or later. The subsytem may move from one microscopic configuration with energy density $e = \langle \mathcal{E} \rangle / N$ to another microscopic configuration with the same energy density through other intermedient configurations of energy density $e$, or through other configurations with energy density $e' \neq e$.

## 1.3 Detailed balance and the microcanonical distribution

Suppose subsystem is at configuration $\mathbf{S}_\alpha(e)$ at time $t$. It will jumps to another configuration $\mathbf{S}_\beta(e)$ at time $t + \Delta t$ with probability $P_{\alpha\to\beta}$. For a macroscopic subsystem at equilibrium, it is usually assumed that there is no net flow in the system. In mathematical terms, this means that

$$P_{\alpha\to\beta} \equiv P_{\beta\to\alpha} \ . \tag{1.3}$$

Equation (1.3) is the so-called detailed balance condition. Notice microscopic configurations $\mathbf{S}_\alpha$ and $\mathbf{S}_\beta$ have the same energy density as that of the mean energy density of the subsystem.

With the assumption of ergodicity and detailed balance, it can be proven that, at equilibrium, a macroscopic subsystem with mean energy density $e$ will stay at each of its miscropic configurations will equal probability. This is the so-called microcanonical distribution:

$$\rho_{\rm mc}(\mathbf{S}(\mathcal{E})) \ = \ \frac{1}{\Omega(Ne)} \qquad \text{for} \quad \mathcal{E}/\mathcal{N} = \langle \mathcal{E} \rangle / \mathcal{N} \ , \tag{1.4}$$

$$= \quad 0 \qquad \text{otherwise} \ . \tag{1.5}$$

In the remaining part of this chapter, for simplicity of discussion, we assume the energy of the subsystem is always equal to its average value and denote this value just as $\mathcal{E}$.

## 1.4 Temperature

The temperature is a measure of the thermal motion intensity of a subsystem. We can define the temperature $T$ of a macroscopic subsystem by many ways which are mutually equivalent to each other as long as the number of particles $\mathcal{N}$ in the subsystem is very huge ($\mathcal{N} \gg 10^{23}$). Here we give the following mathematical definition

$$\frac{1}{T} = k_{\rm B} \frac{{\rm d} \ln \Omega(\mathcal{E})}{{\rm d}\mathcal{E}} \ , \tag{1.6}$$

where $\mathcal{E}$ is the (average) energy of the subsystem as discussed in the preceding section; and $k_{\rm B} = 1.38 \times 10^{-23}\ J/K$ is Boltzmann's constant.

We can also define $\mathcal{S}(\mathcal{E}) = k_{\rm B} \ln \Omega(\mathcal{E})$ as the entropy of the subsystem (see also Sec. 1.8). Then Eq. (1.6) can be re-written as $T^{-1} = {\rm d}\mathcal{S}(\mathcal{E})/{\rm d}\mathcal{E}$.

As a simple example, let us consider the case of very weakly interacting gas (or ideal gas) which is confined in a $d$-dimensional cubic box of volume $V$. The total number of gas particles is $\mathcal{N}$. The total energy $\mathcal{E}$ of the ideal gas subsystem is

$$\mathcal{E} = \sum_{i=1}^{\mathcal{N}} E_i = \sum_{i=1}^{\mathcal{N}} \frac{\mathbf{p}_i^2}{2m} \ , \tag{1.7}$$

where $\mathbf{p}_i$ is the momentum of a gas particle and $m$ is its mass. The mean energy of the subsystem is regarded as fixed. Then the total number of configurations of the subsystem is

$$\begin{aligned} \Omega(\mathcal{E}) &= \frac{1}{\hbar^{\mathcal{N}} \mathcal{N}!} \prod_{i=1}^{\mathcal{N}} \int {\rm d}\mathbf{r}_{\rm i} {\rm d}\mathbf{p}_{\rm i} \delta(\mathcal{E} - \sum_{\rm i} \frac{\mathbf{p}_{\rm i}^2}{2{\rm m}}) \\ &= \frac{1}{\hbar^{\mathcal{N}} \mathcal{N}!} V^{\mathcal{N}} \frac{2\pi^{\frac{d\mathcal{N}}{2}}}{\Gamma(\frac{d\mathcal{N}}{2})} (2m\mathcal{E})^{\frac{d\mathcal{N}-1}{2}} \ . \end{aligned} \tag{1.8}$$

Inserting Eq. (1.8) into Eq. (1.6), we get that

$$\frac{1}{T} = \frac{d\mathcal{N}-1}{2} \frac{k_{\rm B}}{\mathcal{E}} \quad \Longrightarrow \quad \mathcal{E} = \frac{d\mathcal{N}-1}{2} k_{\rm B} T \simeq \mathcal{N} \frac{d}{2} k_{\rm B} T \ . \tag{1.9}$$

## 1.5 Boltzmann distribution

Let us in turn consider a subsystem (see Fig. 1.2) of the macroscopic subsystem that has been discussed in Sec. 1.1–1.4. This sub-subsystem is the physical system of our real interest (and we just referred to it as the physical system). This physical system contains a total number of $N$ particles, where $N$ is also a large number but with $N \ll \mathcal{N}$, the size of the subsystem.

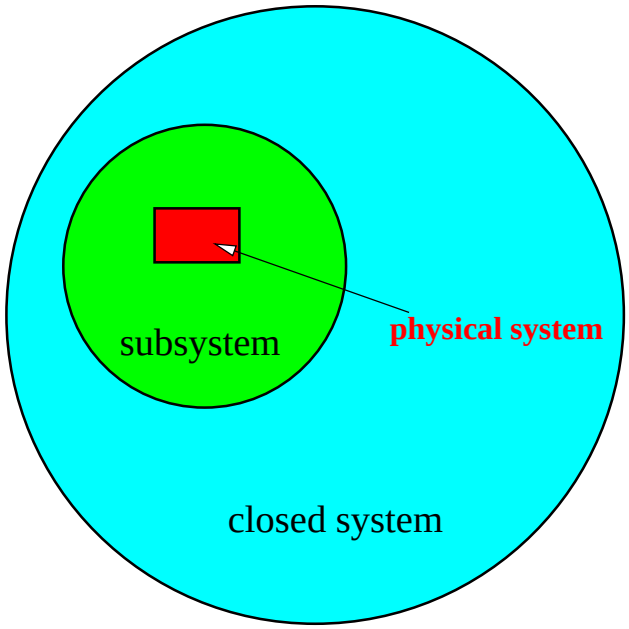


Figure 1.2: A physical system (as denoted by the rectangular box) of interest. This physical system is inside a large macroscopic subsystem which serves as the thermal bath with constant temperature $T$.

The energy of the whole subsystem is

$$\mathcal{E}(\mathbf{s}, \mathbf{S}') = E(\mathbf{s}) + \mathcal{E}'(\mathbf{S}') + \Delta E(\mathbf{s}, \mathbf{S}') \ . \tag{1.10}$$

In Eq. (1.10), $E$ is the internal energy of the physical system, which is a function of the microscopic configuration $\mathbf{s}$ of the physical system only; $\mathcal{E}'$ is the energy of the remaining part of the subsystem and $\mathcal{S}'$ denotes a microscopic configuration of this remaining part; and $\Delta E$ is the interfacial energy between the physical system and the remaining part of the subsystem.

In the general case, the interfacial energy $\Delta E$ can be neglected compared with the internal energy $E$ of the physical system. Then, the probability that the physical system take the particular configuration $\mathbf{s}$ is governed by the Boltzmann distribution

$$\rho(\mathbf{s}) \propto \exp(-\beta E(\mathbf{s})) \ , \tag{1.11}$$

where $\beta = (k_{\rm B}T)^{-1}$ is the Boltzmann factor. Here $T$ is the temperature of the subsystem as defined in Sec. 1.4.

Here we give a heuristic deduction of Eq. (1.11). The reader is advised to consult a standard textbook (e.g., [1]) for a more rigorous understanding of this equation.

According to the micro-canonical distribution Eq. (1.4), each configuration of the subsystem with energy $\mathcal{E}$ is equiprobable. Therefore, the probability that the physical system be in a microscopic state $\mathbf{s}$ is proportional to the total number of configurations $\tilde{\Omega}(\mathcal{E} - E(\mathbf{s}))$ of the remaining part of the subsystem with energy $\mathcal{E} - E(\mathbf{s})$. In other words,

$$\begin{aligned}
\rho(\mathbf{s}) &\propto \tilde{\Omega}(\mathcal{E} - E(\mathbf{s})) && (1.12)\\
&= \exp\Big( \int^{\mathcal{E}-E(\mathbf{s})} \frac{1}{k_{\rm B}T(\tilde{\mathcal{E}})} {\rm d}\tilde{\mathcal{E}} \Big) && (1.13)\\
&= \exp\Big( \int^{\mathcal{E}} \frac{1}{k_{\rm B}T(\tilde{\mathcal{E}})} {\rm d}\tilde{\mathcal{E}} - \int_{\mathcal{E}-{\rm E}(\mathbf{s})}^{\mathcal{E}} \frac{1}{{\rm k_B T}(\tilde{\mathcal{E}})} {\rm d}\tilde{\mathcal{E}} \Big) && (1.14)\\
&= \exp(-\frac{E(\mathbf{s})}{k_{\rm B}T}) \ . && (1.15)
\end{aligned}$$

In writing down Eq. (1.13), we have used Eq. (1.6) and the fact that the subsystem is much larger than the physical system of interest.

A remark: Is the interfacial energy $\Delta E$ in Eq. (1.10) totally un-important in understanding the macroscopic property of a given physical system? The answer might be very subtle. If the physical system has a phase transition, such an interfacial energy might become quite important at the phase transition point. It may even determine the order of the phase transition.

## 1.6 Partition function

The normalization factor of the the Boltzmann distribution Eq. (1.11) is

$$Z(N,T) = \sum_{\mathbf{s}} \exp(-\beta E(\mathbf{s})) \ . \tag{1.16}$$

$Z(N,T)$ is called the partition function. It is a weighted sum over all the microscopic configurations of a physical system.

## 1.7 Free energy

The partition function is connected with the free energy of the physical system by the following very important formula

$$Z(N,T) \equiv \exp\Big(-\beta F(N,T)\Big) \implies F(N,T) \equiv -k_{\rm B}T \ln Z(N,T) \ , \tag{1.17}$$

or, in other words

$$F(N,T) \equiv -k_{\rm B}T \ln\Big(\sum_{\mathbf{s}} e^{-\beta E(\mathbf{s})}\Big) \ . \tag{1.18}$$

Equation (1.18) related the microscopic interactions of the physical system with its macroscopic properties. The left-hand of Eq. (1.18), $F(N,T)$ is a macroscopic thermodynamic quantity; on the other hand, the right-hand side of Eq. (1.18) contains the weighted sum of all the microscopic configurations of the physical system.

Equation (1.17) can be written in another form as

$$\begin{aligned} e^{-\beta F} &= \sum_{E} \Omega(E) e^{-\beta E} = \sum_{E} e^{-\beta E + \ln \Omega(E)} \\ &= N \int {\rm d}\epsilon {\rm e}^{{\rm N}\left(-\beta\epsilon + {\rm s}(\epsilon)/{\rm k_B}\right)} \ , \end{aligned} \tag{1.19}$$

where

$$\epsilon = \frac{E}{N} \tag{1.20}$$

is the energy density of the physical system; and

$$s(\epsilon) = k_{\rm B} \frac{\ln \Omega(N\epsilon)}{N} \tag{1.21}$$

is the entropy density of the physical system at given energy energy density $\epsilon$.

When $N \to \infty$ (the so-called thermodynamic limit), Eq. (1.19) indicates that the free energy density is

$$f(T) \equiv \lim_{N\to\infty} \frac{F(N,T)}{N} = \min_{\epsilon}[\epsilon - Ts(\epsilon)] \ . \tag{1.22}$$

Equation (1.22) indicates that, at given environmental temperature $T$, the macroscopic property of a physical system is determined mainly by those macroscopic configurations whose energy density $\epsilon$ is at the minimum point of $\epsilon - Ts(\epsilon)$.

The mean internal energy of the physical system is

$$\langle E\rangle = \sum_s E(\mathbf{s})\rho(\mathbf{s}) = \sum_{\mathbf{s}} \frac{E(\mathbf{s})e^{-\beta E(\mathbf{s})}}{Z(N,T)} = -\frac{\partial \ln Z}{\partial \beta} = F + \beta\frac{\partial F}{\partial \beta} \ . \tag{1.23}$$

## 1.8 Entropy

The entropy of a physical system is a measure of its disorder at given temperature $T$. It can be defined by the following mathematical formula

$$S(T) = -k_{\rm B}\sum_{\mathbf{s}} \rho(\mathbf{s}) \ln \rho(\mathbf{s}) \ . \tag{1.24}$$

In information science, this definition is called the information entropy: it measures the amount of information needed to fully describe a system.

From Eq. (1.24) it is easy to derive that

$$S(T) = \frac{\langle E\rangle - F}{T} \tag{1.25}$$

or, equivalently,

$$F(T) = \langle E\rangle - TS(T) \ . \tag{1.26}$$

In the thermodynamic limit of $N \to \infty$, Eq. (1.26) is equivalent to Eq. (1.22). This is because $S(T) = k_{\rm B} \ln \Omega(\langle E(T)\rangle)$ in this limit.

## 1.9 Fluctuations

The fluctuations of a thermodynamic quantity can be calculated by differentiation of the partition function. For example,

$$\langle E^2 \rangle - \langle E \rangle^2 = \frac{\partial^2 \ln Z(N,T)}{\partial \beta^2} = -2\frac{\partial F}{\partial \beta} - \frac{\partial^2 F}{\partial \beta^2} \ . \tag{1.27}$$

Comparing Eq. (1.27) with Eq. (1.23), we see that the fluctuation of an extensive quantity (such as the internal energy $E$) is of the same order as the mean value of this extensive quantity.

# Chapter 2

# Mean-Field Models of Phase Transition

Phase transition is a central topic of equilibrium statistical physics. The existence of a phase transition means the system under study has some sort of singularity at the phase transition point, i.e., a minute variation in the control parameter (such as temperature, magnetic field, presure, external force, ect.) results in a dramatic change in the system's macroscopic behavior. The most frequently encountered phase transition in our every day life might be the liquid–vapor transition of water at 100 °C.

Phase transitions can be divided into two general types: continuous phase transitions and discontinuous (first-order) phase transitions. In terms of free energy density, the distinctions between these twe types of phase transitions are shown schematically in Fig. 2.1 for some mean-field models.

At the vicinity of a continuous phase transition, there is large fluctuations in the order parameter. On the other hand, metastable states and hysterisis are usually observed for systems with a dis-continuous phase transition. In a finite-dimensional system, a metastable state is not thermodynamically stable. This means that in the height of the free energy barrier between a metastable state and a state of globule minimum free energy density is finite even for an infinite system. This can be understood as follows. We denote the free energy density of an equilibrium state by $f$, and that of a metastable state by $f + \delta f$ with $\delta f > 0$. Initially the system is supposed to be in the metastable state. Now we perform a perturbation to the system such that, inside the system a $d$-dimensional sphere of radius $r$ is in the equilibrium

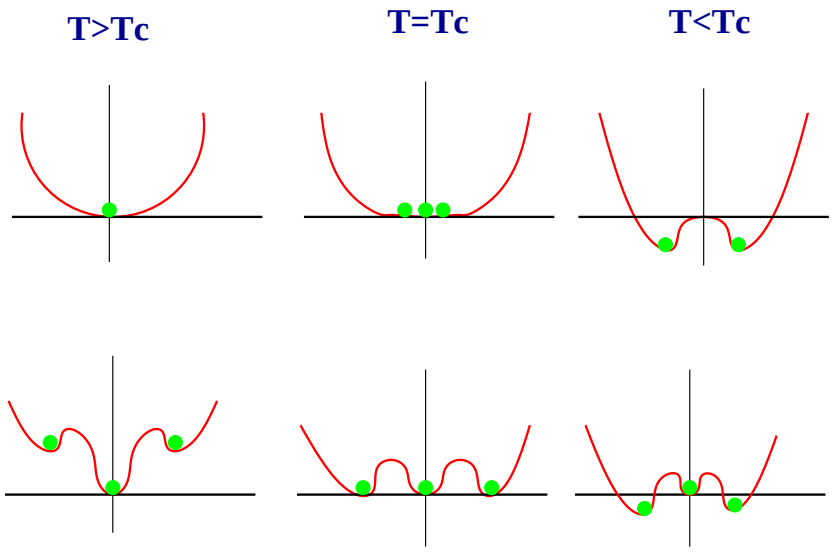


Figure 2.1: Free energy density value (vertical axis) as a function of the value of a general order parameter (horizontal axis) at temperatures above, equaling, or below the phase transition temperature $T_c$. (Top panel) continuous phase transition. (Bottom panel) first-order phase transition in an infinte-dimensional system.

state. The change in the free energy of the system is

$$-c_1 r^d \delta f + c_2 r^{d-1} \delta f' \ , \tag{2.1}$$

where $c_1$ and $c_2$ are two numerical constants, and $\delta f'$ is a positive free energy density due to surface interactions. The first term of Eq. (2.1) comes from volume effect and the second term of Eq. (2.1) comes from surface effect. Equation (2.1) indicates that the free energy barrier between the metastable state and the equilibrium state is of the order const $\times (\delta f)^{-d+1}$. This barrier is finite as long as $\delta f > 0$. It becomes infinite only at the phase transition point. (For an infinite-dimensional model system, the free energy barrier between a metastable state and the true equilibrium state can be infinite, however. This will become more clear in later models.)

Among continuous phase transitions, the second-order phase transition is of the most importance. In what follows we study in some detail four exactly solvable models to illustrate the concepts of first-order and second-order phase transitions.

We mention not at all the renormalization group approach to phase transitions. The interested reader is referred to stardard text books (e.g., [3, 4]).

## 2.1 Infinite-dimensional Ising model with two-body interactions

The model Hamiltonian is

$$H(\sigma) = -\frac{J_0}{N} \sum_{1 \le i < j \le N} \sigma_i \sigma_j \ , \tag{2.2}$$

$\sigma \equiv \{\sigma_1, \sigma_2, \ldots, \sigma_N\}$ is a spin configuration with $\sigma_i \in \{-1, +1\}$; $N$ is the total number of vertices in the system; and $J_0/N$ is the coupling constant between two vertices.

The partition function of the model is

$$\begin{aligned} Z(N) &= \sum_{\sigma} e^{-\beta H(\sigma)} = e^{-\beta J_0/2} \sum_{\sigma} e^{N(\beta J_0/2)(\sum_i \sigma_i/N)^2} \\ &= e^{-\beta J_0/2} \sum_{q} \frac{N!}{(N(1+q)/2)!(N(1-q)/2)!} e^{N\beta J_0 q^2/2} \\ &= e^{-\beta J_0/2} \int_{-1}^{1} \mathrm{d}q \frac{2}{(2\pi N(1-q^2))^{1/2}} \times \\ &\quad \exp\Big(N[-\frac{1+q}{2}\ln\frac{1+q}{2} - \frac{1-q}{2}\ln\frac{1-q}{2} + \frac{\beta J_0 q^2}{2}]\Big) \ . \end{aligned} \tag{2.3}$$

In Eq. (2.3), the parameter $q = \sum_i \sigma_i/N$ is the overlap of a spin pattern $\sigma$ with the spin-all-up pattern.

The free energy density of the system is

$$\begin{aligned} f_{\mathrm{Ising}}^{2\infty} &= -\lim_{N\to\infty} \frac{1}{N\beta} \ln Z(N) \\ &= \min_{-1<q<1} \Big[ -\frac{J_0 q^2}{2} + T\frac{1+q}{2}\ln\frac{1+q}{2} + T\frac{1-q}{2}\ln\frac{1-q}{2} \Big] \ . \end{aligned} \tag{2.4}$$

Figure 2.2 shows the value of the expression in the square brackets of Eq. (2.4) as a function of the overlap $q$. When the temperature $T > J_0$, the minimal free energy density of Eq. (2.4) is located at $q = 0$; the system is in the

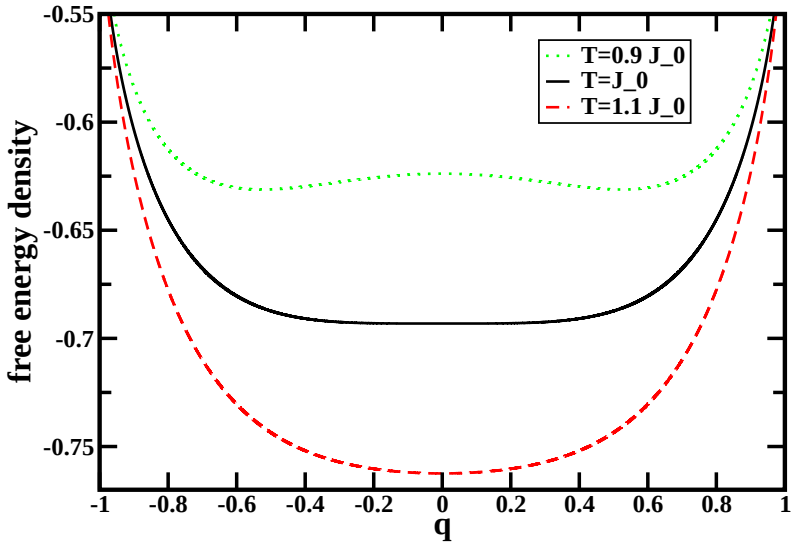


Figure 2.2: The free energy density of the infinite dimensional Ising model as a function of the overlap $q$ for different temperatures.

paramagnetic phase with no spontaneous magnetization. When $T < J_0$, the minimal free energy density of Eq. (2.4) is located at $q = \pm q_0(T) \neq 0$; the system is in the ferromagnetic phase, with spontaneous magnetization. The paramagnet–ferromagnet phase transition occurs at $T = T_c = J_0$. This phase transition is a continuous phase transition, since the order parameter $q_0(T)$ deviates from zero continuously as $T$ is decreased below $T_c$. Actually, at the vicinity of $T = T_c$, there is the following scaling relation:

$$q_0(T) \propto (T_c - T)^{1/2} \qquad (0 < T_c - T \ll T_c) \tag{2.5}$$

Furthermore, the susceptibility of the system approaches infinity at the transition point:

$$\chi = \left.\frac{\partial q_0(T,h)}{\partial h}\right|_{h=0} \propto |T - T_c|^{-1/2} \qquad (|T - T_c| \ll T_c) \tag{2.6}$$

## 2.2 Infinite dimensional Ising model with many-body interactions

The model Hamiltonian is

$$H(\sigma) = -\frac{J_0}{N^{p-1}} \sum_{i_1,i_2,\ldots,i_p} \sigma_{i_1}\sigma_{i_2}\ldots\sigma_{i_p} \ , \tag{2.7}$$

The free energy density of this system is

$$f_{\rm Ising}^{p\infty} = \min_{-1<q<1}\Big[-\frac{J_0 q^p}{p!} + T\frac{1+q}{2}\ln\frac{1+q}{2} + T\frac{1-q}{2}\ln\frac{1-q}{2}\Big] \ . \tag{2.8}$$

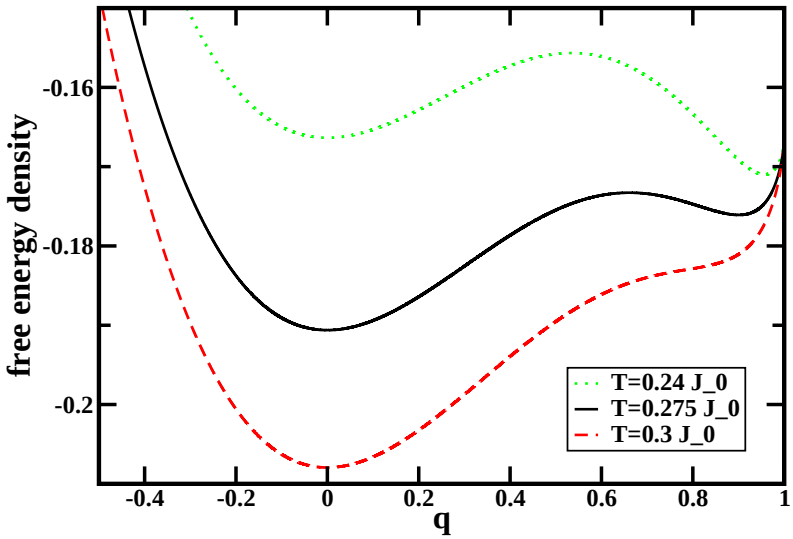


Figure 2.3: The free energy density of the infinite dimensional Ising model with three-body interaction as a function of the overlap $q$ for different temperatures.

As an example, let us consider the case of $p = 3$ (three-body interaction). Figure 2.3 shows the value of the expression in the square brackets of Eq. (2.8) as a function of the overlap $q$. When the temperature $T > 0.2914J_0$, the minimal free energy density of Eq. (2.4) is located at $q = 0$; the system

is in the paramagnetic phase with no spontaneous magnetization. When $0.2480J_0 < T < 0.2914J_0$, the minimal free energy density is still located at $q = 0$; however, a metastable state with $q \simeq 0.95$ appears. When $T < 0.2480J_0$, the minimal free energy density is located at $q \simeq 0.95$ and the state at $q \simeq 0$ becomes metastable. In this parameter regime, the system is in the ferromagnetic phase with non-zero spontaneous magnetization. This phase transition is a dis-continuous one, since the order parameter jumps at the phase transition point $T_c \simeq 0.2480J_0$.

# Chapter 3

# The Bethe-Peierls Approximation and the Cavity Method

There are in general two types of mean-field methods to study finite-connectivity Ising model on a regular lattice. One is the Bragg-Williams approximation, and the other is the Bethe-Peierls approximation [5]. The Bragg-Williams approximation is discussed thoroughly in textbooks of statistical physics; on the other hand, the idea of Bethe-Peierls approximation appears to be less frequently mentioned. Here we describe the basic idea of the Bethe-Peierls approximation in some detail by working on an exactly solvable finite-connectivity model.

## 3.1 Ising model on a random regular graphs

We study the Ising model on a random regular graph $G_K$. The graph has $N$ vertices and $M = NK/2$ edges which connect pairs of vertices. Each vertex of graph $G_K$ is connected by $K$ edges to other vertices of the graph. The graph is otherwise completely random [6]. Denote $E(G_K)$ as the edge set of graph $G_K$.

Each vertex of the graph has a spin state $\sigma_i \in \{-1, +1\}$. Each spin configuration of the system $\vec{\sigma}_N \equiv \{\sigma_1, \sigma_2, \ldots, \sigma_N\}$ is associated with an energy

$$H(\vec{\sigma}_N) = -J_0 \sum_{(i,j)\in E(G_K)} \sigma_i \sigma_j \ , \tag{3.1}$$

where $J_0$ is a coupling constant.

At this point, let us define the concept of cavity graphs [7, 8]. For the present system, a cavity graph of $N$ vertices is also a completely random graph. Among its $N$ vertices, $m$ ($\ll N$) of which have vertex degree $K-1$ [see Fig. 3.1 (left)], while all the other vertices have vertex degree $K$. These $m$ vertices of degree $K-1$ are referred to as the cavity vertices of this cavity graph.

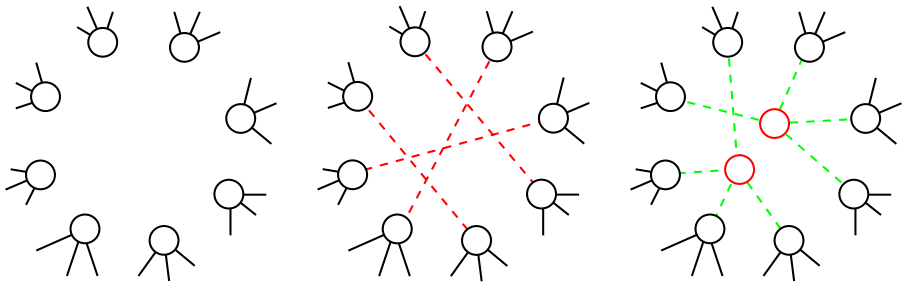

Figure 3.1: The cavity approach to the Ising model Eq. (3.1) on a random regular graph of connectivity $K \equiv 4$. (Left) A part of a cavity graph with $2K$ cavity vertices. (Middle) Construction of a random regular graph of size $N$ from a cavity graph with $2K$ cavity vertices. (Right) Construction of a random regular graph of size $N+2$ from a cavity graph of $2K$ cavity vertices.

At temperature $T$, the spins on each vertex of the cavity graph certainly will fluctuate over time. Denote $P(\sigma_{i_1}, \sigma_{i_2}, \ldots, \sigma_{i_m})$ as the joint probability distribution of the spin values on $m$ cavity vertices $\sigma_{i_1}, \sigma_{i_2}, \ldots, \sigma_{i_m}$ of a cavity graph. In a random graph, the shortest path length between any two randomly chosen vertices scales with the graph size $N$ logarithmically ($\sim \ln N$). As the zeroth-order approximation, we may assume that $P(\sigma_{i_1}, \sigma_{i_2}, \ldots, \sigma_{i_m})$ can be written as the following factorized form

$$P(\sigma_{i_1}, \sigma_{i_2}, \ldots, \sigma_{i_m}) \simeq \prod_{s=1}^{m} P(\sigma_{i_s}) = \prod_{s=1}^{m} (\rho_{i_s}^{+} \delta_{\sigma_{i_s}}^{+1} + \rho_{i_s}^{-} \delta_{\sigma_{i_s}}^{-1}) \ . \tag{3.2}$$

In Eq. (3.2), $P(\sigma_{i_s}) = \rho_{i_s}^{+} \delta_{\sigma_{i_s}}^{+1} + \rho_{i_s}^{-} \delta_{\sigma_{i_s}}^{-1}$ is the marginal distribution of the spin value $\sigma_{i_s}$ of the cavity vertex $i_s$, where $\rho_{i_s}^{+} + \rho_{i_s}^{-} \equiv 1$. Equation (3.2) is the Bethe-Peierls approximation. It assumes statistical independence among the spin states of the cavity vertices.

To write down a self-consistent equation for the marginal probability $P(\sigma_i)$, we notice that a cavity vertex $i$ in a graph of size $N$ can be obtained by the following way: First, generate a cavity graph of $N-1$ vertices and $K-1$ cavity vertices; then, add a new vertex $i$ and connect it to the $K-1$ cavity vertices. Denote $\partial i$ as the nearest neighbors of vertex $i$ in the new graph. The partition function of the cavity vertex $i$ is

$$z_i = \sum_{\sigma_i} \sum_{\sigma_j : j \in \partial i} P(\{\sigma_j\}) \exp\Big( \beta J_0 \sigma_i \sum_{j \in \partial i} \sigma_j \Big) \tag{3.3}$$

If we insert the factorized form Eq. (3.2) into Eq. (3.3), we obtain that

$$z_i = \prod_{j \in \partial i} (\rho_j^+ e^{\beta J_0} + \rho_j^- e^{-\beta J_0}) + \prod_{j \in \partial i} (\rho_j^+ e^{-\beta J_0} + \rho_j^- e^{\beta J_0}) \tag{3.4}$$

Then, the probability that vertex $i$ takes the postive spin value is

$$\rho_i^+ = \frac{\prod\limits_{j \in \partial i} (\rho_j^+ e^{\beta J_0} + \rho_j^- e^{-\beta J_0})}{\prod\limits_{j \in \partial i} (\rho_j^+ e^{\beta J_0} + \rho_j^- e^{-\beta J_0}) + \prod\limits_{j \in \partial i} (\rho_j^+ e^{-\beta J_0} + \rho_j^- e^{\beta J_0})} \ . \tag{3.5}$$

A homogenous fixed-point solution of Eq. (3.5) is given by

$$\rho_{\rm cv}^+ = \frac{(\rho_{\rm cv}^+ e^{\beta J_0} + (1-\rho_{\rm cv}^+) e^{-\beta J_0})^{K-1}}{(\rho_{\rm cv}^+ e^{\beta J_0} + (1-\rho_{\rm cv}^+) e^{-\beta J_0})^{K-1} + (\rho_{\rm cv}^+ e^{-\beta J_0} + (1-\rho_{\rm cv}^+) e^{\beta J_0})^{K-1}} \ . \tag{3.6}$$

We can also perform population dynamics iteration (see, e.g., [9]) to find a steady state probability distribution of $\rho_i^+$ over all the (cavity) vertices of a very large random regular graph. We found that this steady state population dynamics solution converges to the stable fixed point of Eq. (3.6).

At equilibrium, the probability that a randomly chosen vertex of a randoum regular graph to be in the spin state $+1$ is then

$$\rho^+ = \frac{(\rho_{\rm cv}^+ e^{\beta J_0} + (1-\rho_{\rm cv}^+) e^{-\beta J_0})^{K}}{(\rho_{\rm cv}^+ e^{\beta J_0} + (1-\rho_{\rm cv}^+) e^{-\beta J_0})^{K} + (\rho_{\rm cv}^+ e^{-\beta J_0} + (1-\rho_{\rm cv}^+) e^{\beta J_0})^{K}} \ . \tag{3.7}$$

The spontaneous magnetization of the system is $\langle m \rangle = 2\rho^+ - 1$.

For the case of $K = 4$, the spontaneous magnetizationn $\langle m \rangle$ as a function of temperature $T$ is shown in Fig. 3.2, while the insert of Fig. 3.2 shows the value of $\rho_{\rm cv}^+$ as a function of temperature. At high temperatures $T \geq 2.886 J_0$,

the only stable solution of Eq. (3.6) is $\rho_{\rm cv}^{+} = 1/2$, i.e., the system is in the paramagnetic phase, without any spontaneous magnetization. As the temperature is lowered to $T < 2.886 J_0$, the order parameter $\rho_{\rm cv}^{+}$ deviates from $1/2$ gradually. In this later temperature region, the system is in the ferromagnetic phase, with non-zero spontaneous magnetization. A paramagnet–ferromagnet phase transition occurs at the critical temperature $T \simeq 2.886 J_0$. This phase transition is continuous (second-order).

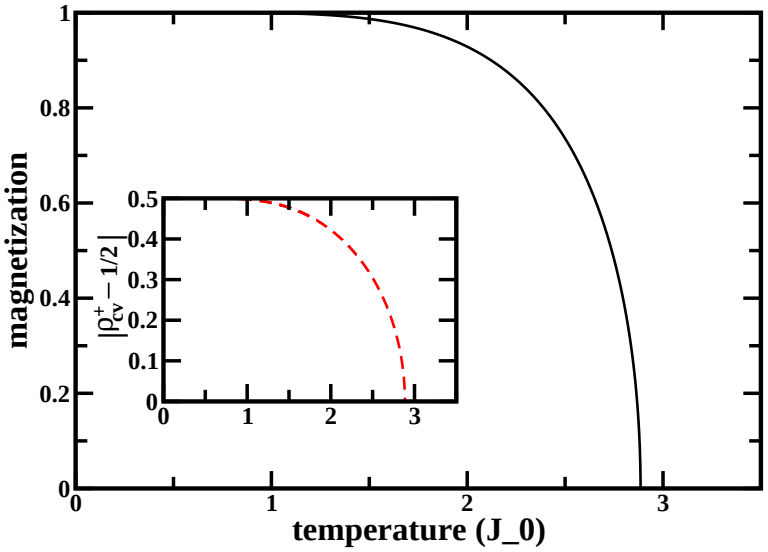


Figure 3.2: Magnetization of the Ising model on a random regular graph with connectivity $K \equiv 4$. (Inset) the value of the order parameter $\rho_{\rm cv}^{+}$ as a function of temperature.

### 3.1.1 Energy density and entropy density

We now calculate the energy density and entropy density of the Ising model Eq. (3.1) through the cavity approach [7, 8]. The energy density is denoted as $\epsilon(K, T)$, while the entropy density of the system at energy density $\epsilon$ is denoted as $\Sigma(K, \epsilon)$.

Denote a random cavity graph with $N$ vertices and $2K$ cavity vertices as $G_{\rm cv}(N)$. According to Fig. 3.1 (middle), a random regular graph $G_K(N)$ of $N$ vertices can be obtained from such a cavity graph $G_{\rm cv}(N)$. One simply

forms $K$ pairs of vertices from the $2K$ cavity vertices of graph $G_{\rm cv}(N)$ and then set up an edge between each formed pair of vertices. Denote the energy of the cavity graph $G_{\rm cv}(N)$ as $H_{\rm cv}(N)$ and $\Delta E_1$ as the difference between the energy of graph $G_K(N)$ and that of graph $G_{\rm cv}(N)$. Then we have the following equation concerning the average values of these energies

$$N\epsilon(K,T) = \langle H_{\rm cv}(N)\rangle + \langle \Delta E_1\rangle \ . \tag{3.8}$$

The energy difference $\Delta E_1$ is expressed as

$$\Delta E_1 = -J_0 \sum_{(i,j)\in e_1} \sigma_i\sigma_j \ , \tag{3.9}$$

where $e_1$ denotes the set of newly added edges in going from $G_{\rm cv}(N)$ to $G_K(N)$. To calculate the average of $\Delta E_1$, we consider the subgraph containing the $2K$ cavity vertices $(i_1, i_2, \ldots, i_{2K})$ of the cavity graph $G_{\rm cv}(N)$ as well as the edge set $e_1$. The partition function of this subgraph is

$$Z_{2K} = \sum_{\sigma_{i_1},\ldots,\sigma_{i_{2K}}} P(\sigma_{i_1},\ldots,\sigma_{i_{2K}}) \exp(-\beta\Delta E_1) \ . \tag{3.10}$$

If we insert the factorized form Eq. (3.2) of $P(\sigma_{i_1},\ldots,\sigma_{i_{2K}})$ into Eq. (3.10), we finally obtain that

$$Z_{2K} = \prod_{(i,j)\in e_1} \Big[(\rho_i^+\rho_j^+ + \rho_i^-\rho_j^-)e^{\beta J_0} + (\rho_i^+\rho_j^- + \rho_i^-\rho_j^+)e^{-\beta J_0}\Big] \ . \tag{3.11}$$

Consequently, we have

$$\langle \Delta E_1\rangle = -\frac{\partial \ln Z_{2K}}{\partial\beta} \tag{3.12}$$

$$= -J_0 \sum_{(i,j)\in e_1} \frac{(\rho_i^+\rho_j^+ + \rho_i^-\rho_j^-)e^{\beta J_0} - (\rho_i^+\rho_j^- + \rho_i^-\rho_j^+)e^{-\beta J_0}}{(\rho_i^+\rho_j^+ + \rho_i^-\rho_j^-)e^{\beta J_0} + (\rho_i^+\rho_j^- + \rho_i^-\rho_j^+)e^{-\beta J_0}} \ . \tag{3.13}$$

For the Ising model on the graph $G_K(N)$, the number of configurations at energy density $\epsilon$ is $\Omega_{G_K}(N\epsilon) = \exp(N\Sigma(K,\epsilon))$. Concerning the entropy density $\Sigma(K,\epsilon)$ of graph $G_K(N)$, we have the following equation [7, 8]

$$\exp\Big(N\Sigma(K,\epsilon)\Big) = \int \exp\Big(N\Sigma_{\rm cv}(\epsilon - \Delta E_1/N)\Big){\rm Prob}(\Delta E_1){\rm d}\Delta E_1 \ , \tag{3.14}$$

where $\Sigma_{\rm cv}(\epsilon')$ is the entropy density of the cavity graph $G_{\rm cv}(N)$ at energy density $\epsilon'$. In Eq. (3.14), Prob($\Delta E_1$) is the (un-reweighted) probability that, after the $K$ edges in the edge set $e_1$ are added, the energy increase in the system is $\Delta E_1$. The expression for this probability is

$$\mathrm{Prob}(\Delta E_1) = \sum_{\{\sigma_i,\sigma_j:(i,j)\in e_1\}} \prod_{(i,j)\in e_1} P(\sigma_i)P(\sigma_j)\delta\Big(\Delta E_1 + J_0 \sum_{(i,j)\in e_1} \sigma_i\sigma_j\Big) \ . \tag{3.15}$$

From Eq. (3.14), we then obtain that

$$\begin{aligned} N\Sigma(K,\epsilon) &= N\Sigma_{\rm cv}(\epsilon) + \ln\Big(\int e^{-\frac{\partial\Sigma_{\rm cv}(\epsilon)}{\partial\epsilon}\Delta E_1}\mathrm{Prob}(\Delta E_1)\mathrm{d}\Delta E_1\Big) & (3.16)\\ &= N\Sigma_{\rm cv}(\epsilon) + \ln\Big(\int e^{-\beta\Delta E_1}\mathrm{Prob}(\Delta E_1)\mathrm{d}\Delta E_1\Big) \ . & (3.17)\end{aligned}$$

In going from Eq. (3.16) to Eq. (3.17), we have used the condition that, when the energy density $\epsilon$ in Eq. (3.16) is equal to the equilibrium energy density of the system, then

$$\beta = \frac{\partial\Sigma_{\rm cv}(\epsilon)}{\partial\epsilon} \tag{3.18}$$

According to Fig. 3.1 (right), a random regular graph $G_K(N+2)$ with $N+2$ vertices can be obtained from a cavity graph $G_{\rm cv}(N)$ of $N$ vertices and $2K$ cavity vertices. This is achieved by adding two new vertices ($i = N+1, N+2$) and connect each of them to $K$ cavity vertices of $G_{\rm cv}(N)$. Similar to Eq. (3.8), we can write down the following equation concerning the change in the energy of the system

$$(N+2)\epsilon(K,T) = \langle H_{\rm cv}(N)\rangle + \langle\Delta E_2\rangle \ , \tag{3.19}$$

where

$$\Delta E_2 = -J_0 \sum_{i=N+1}^{N+2}\sum_{j\in\partial i}\sigma_i\sigma_j \tag{3.20}$$

is the energy increase caused by the addition of the two new vertices. The partition function $Z_{2K+2}$ for the subraph involving the two new vertices and their nearest neighbors can easily be written down. The final result reads

$$Z_{2K+2} = z_{N+1}z_{N+2} \ , \tag{3.21}$$

where $z_i$ is given by Eq. (3.3). Similar to Eq. (3.13), we find that

$$\langle \Delta E_2 \rangle = -\frac{\partial \ln Z_{2K+2}}{\partial \beta} = -\frac{\partial \ln z_{N+1}}{\partial \beta} - \frac{\partial \ln z_{N+2}}{\partial \beta} \tag{3.22}$$

$$\begin{aligned} &= -J_0 \sum_{i=N+1}^{N+2} \frac{\sum\limits_{j\in\partial i} \frac{\rho_j^+ e^{\beta J_0} - \rho_j^- e^{-\beta J_0}}{\rho_j^+ e^{\beta J_0} + \rho_j^- e^{-\beta J_0}} \prod\limits_{k\in\partial i} (\rho_k^+ e^{\beta J_0} + \rho_k^- e^{-\beta J_0})}{\prod\limits_{k\in\partial i} (\rho_k^+ e^{\beta J_0} + \rho_k^- e^{-\beta J_0}) + \prod\limits_{k\in\partial i} (\rho_k^+ e^{-\beta J_0} + \rho_k^- e^{\beta J_0})} \\ &\quad + J_0 \sum_{i=N+1}^{N+2} \frac{\sum\limits_{j\in\partial i} \frac{\rho_j^+ e^{-\beta J_0} - \rho_j^- e^{\beta J_0}}{\rho_j^+ e^{-\beta J_0} + \rho_j^- e^{\beta J_0}} \prod\limits_{k\in\partial i} (\rho_k^+ e^{-\beta J_0} + \rho_k^- e^{\beta J_0})}{\prod\limits_{k\in\partial i} (\rho_k^+ e^{\beta J_0} + \rho_k^- e^{-\beta J_0}) + \prod\limits_{k\in\partial i} (\rho_k^+ e^{-\beta J_0} + \rho_k^- e^{\beta J_0})} \ . \end{aligned} \tag{3.23}$$

Combining Eqs. (3.8) and (3.19), we obtain the following expression for the energy density of the system

$$\epsilon(K,T) = \frac{1}{2}\langle \Delta E_2 \rangle - \frac{1}{2}\langle \Delta E_1 \rangle \ . \tag{3.24}$$

Similar to Eq. (3.17), the entropy of the graph $G_K(N+2)$ is expressed as

$$(N+2)\Sigma(K,\epsilon) = N\Sigma_{\rm cv}(\epsilon) + 2\beta\epsilon + 2\ln(2) + \ln\Big(\int e^{-\beta\Delta E_2} {\rm Prob}(\Delta E_2) {\rm d}\Delta E_2\Big) \ , \tag{3.25}$$

where

$${\rm Prob}(\Delta E_2) = \frac{1}{4} \prod_{i=N+1}^{N+2} \Big[\sum_{\sigma_i} \sum_{\sigma_j : j\in\partial i} \prod_{j\in\partial i} P(\sigma_j)\Big] \delta\Big(\Delta E_2 + J_0 \sum_{i=N+1}^{N+2} \sum_{j\in\partial i} \sigma_i\sigma_j\Big) \ . \tag{3.26}$$

In Eq. (3.25), the term $2\ln(2)$ results from the total number of configurations of the two newly added vertices ($i = N+1, N+2$). Combining Eqs. (3.17) and (3.25), we obtain the following expression for the entropy density of the system

$$\begin{aligned} \Sigma(K,\epsilon) &= \beta\epsilon + \ln(2) + \frac{1}{2}\ln\Big(\int e^{-\beta\Delta E_2} {\rm Prob}(\Delta E_2) {\rm d}\Delta E_2\Big) \\ &\quad -\frac{1}{2}\ln\Big(\int e^{-\beta\Delta E_1} {\rm Prob}(\Delta E_1) {\rm d}\Delta E_1\Big) \ . \end{aligned} \tag{3.27}$$

In the above equation, $\epsilon$ is the energy density of the system at temperature $T$. The free energy density of the system is then

$$f(K,T) = \epsilon(K,T) - T\Sigma(K,\epsilon(K,T)) \ . \tag{3.28}$$

Figure 3.3 shows the equilibrium energy density, entropy density, and free energy density of a Ising model on a random regular graph of $K \equiv 4$. At the paramagnet–ferromagnet transition point $T \simeq 2.886 J_0$, both the energy density and the entropy density have a kink; however, the free energy density and its first-order derivative with respective to temperature are both continuous. This confirms the conclusion that the paramagnet–ferromagnet transition is a continous phase transition.

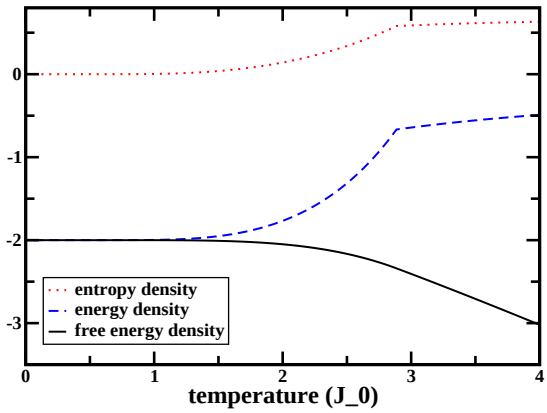


Figure 3.3: Equilibrium entropy density, energy density, and free energy density for the Ising model Eq. (3.1) on a random regular graph with vertex degree $K = 4$. Enegy unit is $J_0$.

## 3.2 $p$-spin interaction Ising model on random regular graphs

In this section we extend the cavity method of the preceding section to more general Ising spin models. Consider a Hamiltonian of the following form

$$H(\vec{\sigma}_N) = \sum_a E_a \ , \tag{3.29}$$

where $E_a$ is the energy associated with an elementary interaction $a$ involving $p$ spins $i_1, i_2, \ldots, i_p$:

$$E_a = -J_0 \sigma_{i_1} \sigma_{i_2} \ldots \sigma_{i_p} = -J_0 \prod_{i \in \partial a} \sigma_i \ . \tag{3.30}$$

In Eq. (3.30), the symbol $\partial a$ denotes the set of spins that are directly involved in the elementary interaction $a$. The model as defined by Eqs. (3.29) and (3.30) can be represented by a factor graph [10] as shown in Fig. 3.4: Each spin of the model system is mapped to a variable node $(i, j, k, \ldots)$, and each interaction is mapped to a function node $(a, b, c, \ldots)$. An edge $(a, i)$ connecting a function node $a$ and a variable node $i$ is created if and only if the spin $\sigma_i$ participates in the interaction $a$. The set of nearest neighbors of a variable node $i$ is denoted as $\partial i$.

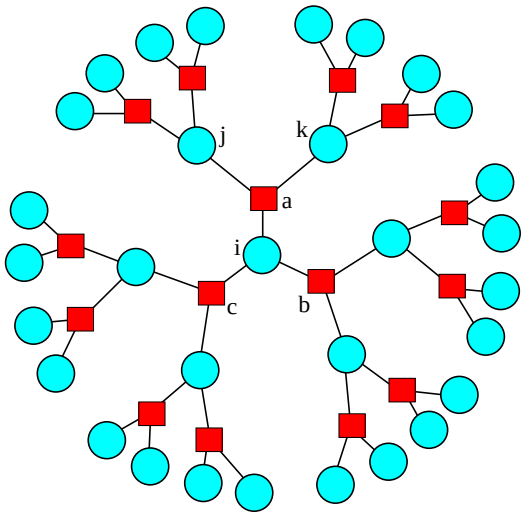


Figure 3.4: Cavity approach to the Ising model with random three-body interactions ($p = 3$) and variable node connectivity $K \equiv 3$. Circles represent variable nodes and squares represent function nodes. The figure shows the neighborhood of variable node $i$.

In this section, we focus on completely random regular factor graphs in which each variable node has $K$ connections and each function node has $p$ connections. To study the statistical physical properties of the $p$-spin interaction Ising model on such a random regular factor graph, we can introduce the concept of cavity factor graphs [7, 8]. A cavity factor graph $G^{(\mathrm{cv})}_{K,p}(N, m)$ is a factor graph with $N$ variable nodes and $(KN - m)/p$ function nodes: (1) among its $N$ variable nodes, $m$ of them have vertex degree $K-1$, while all the others have vertex degree $K$; (2) each function node is connected to $p$ variable nodes; and (3) the graph is randomly connected under the constraints

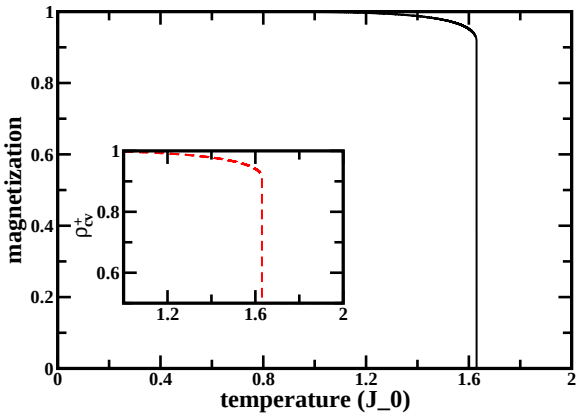


Figure 3.5: Magnetization of an three-body interaction Ising model on a random regular factor graph with connectivity $K \equiv 4$. (Inset) the value of the order parameter $\rho_{\rm cv}^{+}$ as a function of temperature.

(1) and (2). The $m$ variable nodes of degree $K-1$ in graph $G_{K,p}^{(\rm cv)}(N,m)$ are referred to as the $m$ cavity vertices of this cavity factor graph.

To calculate the alighnment probability $\rho_i^+$ that a cavity vertex is in the spin positive state, we can first generate a cavity factor graph $G_{K,p}^{(\rm cv)}(N-1,(p-1)(K-1))$ of $(p-1)(K-1)$ cavity vertices, then we add variable node $i$ and connect it to these old cavity vertices through $K-1$ function nodes. An iteration equation for $\rho_i^+$ can be obtained. For the case of $p=3$, the final fixed-point equation for $\rho_i^+$ is

$$\rho_i^+ \equiv \rho_{\rm cv}^+ = \frac{\Big((1-2\rho_{\rm cv}^+(1-\rho_{\rm cv}^+))e^{\beta J_0}+2\rho_{\rm cv}^+(1-\rho_{\rm cv}^+)e^{-\beta J_0}\Big)^{K-1}}{\sum\limits_{\sigma=\pm 1}\Big((1-2\rho_{\rm cv}^+(1-\rho_{\rm cv}^+))e^{\sigma\beta J_0}+2\rho_{\rm cv}^+(1-\rho_{\rm cv}^+)e^{-\sigma\beta J_0}\Big)^{K-1}}. \tag{3.31}$$

The probability $\rho^+$ for a randomly chosen spin of the model to be positive is then

$$\rho^+ = \frac{\Big((1-2\rho_{\rm cv}^+(1-\rho_{\rm cv}^+))e^{\beta J_0}+2\rho_{\rm cv}^+(1-\rho_{\rm cv}^+)e^{-\beta J_0}\Big)^{K}}{\sum\limits_{\sigma=\pm 1}\Big((1-2\rho_{\rm cv}^+(1-\rho_{\rm cv}^+))e^{\sigma\beta J_0}+2\rho_{\rm cv}^+(1-\rho_{\rm cv}^+)e^{-\sigma\beta J_0}\Big)^{K}}. \tag{3.32}$$

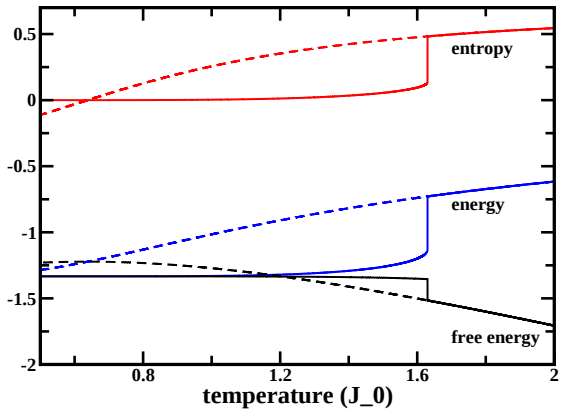


Figure 3.6: Equilibrium entropy density, energy density, and free energy density for the ferromagnetic phase (solid lines) and paramagnetic phase (dashed lines) of the three-body interaction Ising model on a random regular factor graph of $K = 4$. Energy and temperature both are in units of $J_0$.

For the case of $p = 3$ and $K = 4$, Fig. 3.5 shows the behavior of the order parameter $\rho^+_{\rm cv}$ as well as that of the spontaneous magnetization $\langle m\rangle = 2\rho^+ - 1$. Equation (3.31) has a fixed-point solution of $\rho^+_{\rm cv} = 1/2$. This solution is locally stable in the whole temperature regime of $T > 0$; it corresponds to the paramagnetic phase of zero spontaneous magnetization. When the temperature $T$ is less than $1.63J_0$, another stable solution of Eq. (3.31) with $\rho^+_{\rm cv} > 0.9$ appears. This later solution corresponds to the ferromagnetic phase. At $T \leq 1.63J_0$, whether the system is in the paramagnetic phase or in the ferromagnetic phase is not known at the moment. We must compare the free energy densities of these two phases to find the true phase transition point. The paramagnet–ferromagnet phase transition of the present system is discontinuous (first-order).

To calculate the energy density and entropy density from the cavity approach, we can first generate a cavity factor graph $G^{(\rm cv)}_{K,p}(N, p(p-1)K)$ of with $p(p-1)K$ cavity vertices. A factor graph $G_{K,p}(N)$ can be generated from this cavity factor graph by adding $(p-1)K$ new function nodes and then connecting each of these new function nodes to $p$ cavity vertices. On the other hand, a factor graph $G_{K,p}(N+p)$ can also be generated from the cavity factor graph $G^{(\rm cv)}_{K,p}(N, p(p-1)K)$ by adding $p$ new variable nodes as well as

$pK$ new function nodes. The final equilibrium expressions of the enenrgy, entropy, and free energy density are a little bit lengthy, therefore, we do not write down the explicit expressions here. For the case of $K = 4$ and $p = 3$, the energy, entropy, and free energy densities are calculated numerically and shown in Fig. 3.6. From this figure we know that, in the tempreature regime of $1.2066J_0 < T < 1.63J_0$, the free energy density of the ferromagnetic phase is higher than that of the paramagnetic phase. This means that the ferromagnetic phase is only a metastable phase in this temperature regime. An equilibrium paramagnet–ferromagnet phase transition occurs at temperature $T \simeq 1.2066J_0$. Below this temperature, the ferromagnetic phase is the true equilibrium phase, while the paramagnetic phase is only a metastable phase.

## 3.3 Going beyond the Bethe-Peierls approximation

To go beyond the Bethe-Peierls approximation, one should consider the correlations among the cavity vertices, which are caused by loops. For recent development along this line of research, see [11, 12].

# Chapter 4

# Structural Phase Transitions in Macromolecule Systems

As an application of statistical mechanics, in this section we study structural phase transitions in single macromolecules. Three examples will be given, namely the denaturation transition of double-stranded DNA, melting of RNA secondary structures, and the collapse transition of two-dimensional flexible and semiflexible polymers.

## 4.1 Denaturation of double-stranded DNA

DNA is the genetic material of most life forms on the earth. It is a double-stranded polymer made of four nucleotide bases A, T, G, and C (see Fig. 4.1). The two strands are bound together by the formation of hydrogen-bonded base-pairs A-T and G-C. The double-stranded structure is further stabilized by base-pair stacking interactions, which are short-ranged potentials between two adjacent base-pairs [13, 14]. Compared to a covalent bond, a hydrogen bond is very weak. The energy needed to break a hydrogen bond is comparable to thermal energy at room temperature of $T \simeq 300\ K$. Experimentally, it has been known for many years that when a solution of DNA macromolecules is heated to about 80 °C, the base-pairs in the DNA double-helix break up cooperatively and the two DNA strands dissociate from each other to form two separated random coils. This phenomenon is referred to as DNA denaturation [13]. (The two strands of a DNA can also be separated by external stretch [15], but we will not discuss this issue here.)

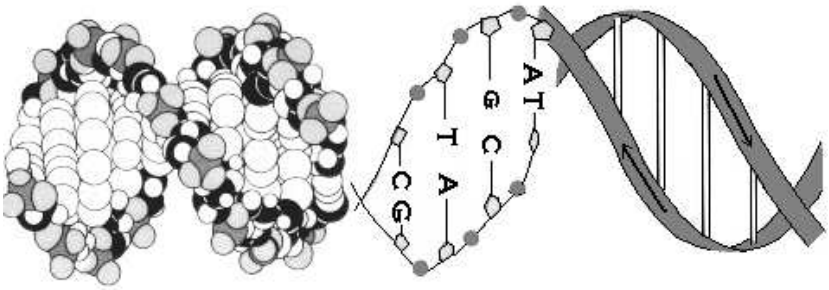


Figure 4.1: local structure of double-stranded DNA.

Here we introduce the Poland-Scheraga model of DNA thermal denaturation [16, 17]. In this model, each base-pair exists either in a base-paired state or in an un-paired open state. A segment of DNA that contains only paired base-pairs is called a double-helical segment, and a segment that is composed completely of opened base-pairs is referred to as a denatured coil segment. DNA could be regarded as a linear chain of double-helical segments and denatured segments, with these two types of segments occur in alternative order (see Fig. 4.2, left panel). When two DNA segments come close together each other, there are excluded volume interactions. Excluded volume interactions also exist between nucleotide bases in a single denatured DNA segment. At first, let us discard any excluded volume effect and focus only on the base-pairing and base-pair stacking interactions. Without loss of generality, we assume the first and the last pair of bases of DNA are always in the paired state. Our purpose is to calculate the free energy density of the system in the limit of infinite long chain length.

Denote the partition function of a DNA double-helical segment of of $n_{\rm h}$ ($n_{\rm h} \geq 1$) base-pairs by $Z_{\rm h}(n_{\rm h})$, and that of a denatured coil segment of $n_{\rm c}$ ($n_{\rm c} \geq 1$) base-pairs as $Z_{\rm c}(n_{\rm c})$. The whole DNA polymer may in the double-helix configuration, or there may be many double-helix segments and denaturation bubbles (see Fig. 4.2, left panel). The total partition function of a DNA of $N$ base-pairs is obtained by summarizing the contributions from all possible configurations [18]:

$$Z(N) = Z_{\rm h}(N) + \sum_{s=1} \sum_{n_{\rm h_0},\ldots,n_{\rm h_s}} \sum_{n_{\rm c_1},\ldots,n_{\rm c_s}} \delta(\sum_{i=0}^{s} n_{\rm h_i} + \sum_{j=1}^{s} n_{\rm c_j}, N) Z_{\rm h}(n_{\rm h_0}) \prod_{m=1}^{s} [Z_{\rm h}(n_{\rm h_m}) Z_{\rm c}(n_{\rm c_m})] \ .$$

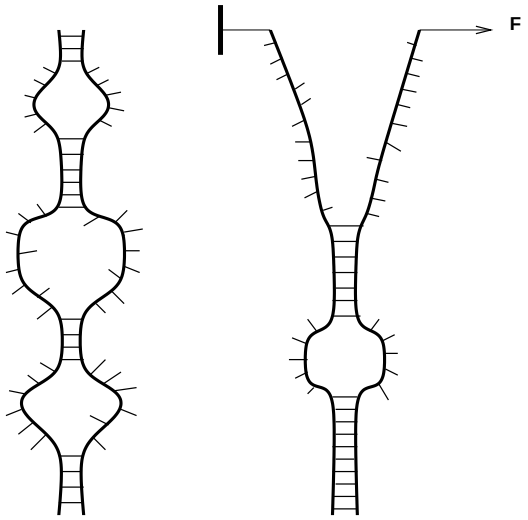


Figure 4.2: DNA denaturation transition. Left panel shows DNA thermal denaturation. Right panel corresponds to force-induced DNA unzipping.

(4.1)

The generating function of Eq. (4.1) is

$$G(z) = \sum_{N=1} Z(N) z^N = \frac{G_{\rm h}(z)}{1 - G_{\rm h}(z) G_{\rm c}(z)} \ . \tag{4.2}$$

In Eq. (4.2), $G_{\rm h}(z)$ and $G_{\rm c}(z)$ are, respectively, the generation function of the partition function of a double-helical segment and a denatured coil segment:

$$G_{\rm h}(z) \ = \ \sum_{n_{\rm h}=1}^{\infty} Z_{\rm h}(n_{\rm h}) z^{n_{\rm h}} \ , \tag{4.3}$$

$$G_{\rm c}(z) \ = \ \sum_{n_{\rm c}=1}^{\infty} Z_{\rm c}(n_{\rm c}) z^{n_{\rm c}} \ . \tag{4.4}$$

For a helical segment of $n_{\rm h}$ base-pairs, the free energy is $-n_{\rm h}\epsilon_{\rm b} - (n_{\rm h}-1)\epsilon_{\rm s}$ due to base-pairing ($\epsilon_{\rm b}$) and base-pair stacking ($\epsilon_{\rm s}$). Therefore

$$G_{\rm h}(z) = \frac{z e^{\beta \epsilon_{\rm b}}}{1 - z e^{\beta(\epsilon_{\rm b} + \epsilon_{\rm s})}} \ . \tag{4.5}$$

The partition function $Z_{\rm c}(n_{\rm c})$ is calculated as follows. A single-stranded DNA segment can be modeled as a freely-jointed chain of bond length $b \simeq 1.7$ nm, with each bond corresponding to about three nucleotide bases. A DNA denaturation bubble of $n_{\rm c}$ base-pairs therefore corresponds to a freely-jointed chain of $2(n_{\rm c}+1)/3$ bonds, with the additional constraint that the two ends of the chain should be separated no more than distance $a$ apart, where $a \simeq 0.3$ nm is the base-pairing interaction range. Then

$$\begin{aligned} Z_{\rm c}(n_{\rm c}) &= \Omega^{2(n_{\rm c}+1)/3} \int\limits_{|\mathbf{R}|\le a} {\rm d}\mathbf{R} \prod_{j=1}^{2(n_{\rm c}+1)/3} [\int {\rm d}\mathbf{t}_{\rm j}/4\pi] \delta(\mathbf{R} - {\rm b} \sum_{\rm l=1}^{2({\rm n_c}+1)/3} \mathbf{t}_{\rm j}) \quad (4.6) \\ &\simeq (2/3\pi)(a/b)^3 \Omega^{2(n_{\rm c}+1)/3} \int\limits_0^\infty p^2 (\frac{\sin p}{p})^{2(n_{\rm c}+1)/3} {\rm dp} \\ &= (6/\pi)^{1/2} (a/b)^3 \Omega^{2(n_{\rm c}+1)/3} (2(n_{\rm c}+1)/3)^{-\gamma} \qquad (\text{for} \quad n_{\rm c} \gg 1) \quad (4.7) \\ &\simeq c_0 \frac{e^{n_{\rm h} s_{\rm c}}}{n_{\rm c}^{\gamma}} \ . \quad (4.8) \end{aligned}$$

In the above equations, $\Omega$ denotes the total number of microscopic configurations of a bond, and $s_{\rm c}$ is the entropy of a single free nucleotide base; the exponent $\gamma = \frac{3}{2}$. The scaling of the partition function of a denaturation bubble with bubble size, $Z_{\rm c}(n_{\rm c}) \propto n_{\rm c}^{-3/2}$, is completely caused by entropic constraint of chain closure. Combining Eq. (4.4) and Eq. (4.8), one observes that the point $z = z_{\rm c} = e^{-s_{\rm c}}$ is the smallest positive singular point of $G_{\rm c}(z)$. At this point, $G_{\rm c}(z_{\rm c})$ is finite but $G'_{\rm c}(z_{\rm c}) \equiv {\rm dG_c/dz}|_{z_{\rm c}}$ is divergent.

Based on Eq. (4.5) and Eq. (4.8), Eq. (4.2) is re-written as

$$G(z) = \frac{z e^{\beta \epsilon_{\rm b}}}{1 - z e^{\beta(\epsilon_{\rm b}+\epsilon_{\rm s})} - z c_0 e^{\beta \epsilon_{\rm b}} \sum_{n_{\rm c}=1}^{\infty} \frac{(z e^{s_{\rm c}})^{n_{\rm c}}}{n_{\rm c}^{3/2}}} \ . \quad (4.9)$$

The free energy density of the system $g(T)$ is related to the partition function by $Z(N) = \exp(-N\beta g(T))$. Then according to Eq. (4.2), the free energy density $g(T)$ is related to the smallest positive sigular point of $G(z)$ through

$$g(T) = k_B T \ln z_0 \ , \quad (4.10)$$

where $z_0$ is the smallest positive singular point of function $G(z)$.

$G(z)$ has two singular points: one is at $z = \exp(-s_{\rm coil})$ and the other is at the point where $1/G(z) = 0$. At low temperatures, the free energy of the

whole system is determined by the second singular point; the system is in the double-helical phase. As temperature is increased, the second singular point approaches the first one, marking the transition from a native DNA into a denatured DNA. The transition is second-order, because at the transition point the free energy density is continuous and its first-order derivative with respect to temperature is also continuous [16, 18].

### 4.1.1 Excluded-volume effect

The above-mentioned model predicts a second-order DNA denaturation transition. However, on the experimental side it is generally believed that DNA denaturation is a first-order phase transition. Therefore, something very significant is still missing in the Poland-Scheraga model.

How will the phase-diagram of DNA denaturation be changed if excluded-volume effect is taken into account? From our preceding discussion, it is obvious that the value of $\gamma$ in Eq. (4.8) could influence the order of the denaturation transition. If $\gamma > 2$ the transition will be first-order, according to Lifson's general argument [18].

Many analytical and computational efforts have been made to include excluded-volume effect in the Poland-Scheraga model. In 1966, Fisher [19] suggested a modified Poland-Scheraga model to include the excluded-volume effect between the two strands of each denaturation bubble. He found that $\gamma \simeq 1.75$ by this modification, so the transition is still second-order. Later on, many theoretical and Monte Carlo simultion investigations (reviewed in [20]) suggested that, when excluded volume effect is fully considered, the DNA denaturation transition should become first-order. For example, Kafri, Mukamel and Peliti [21] in their theoretical work has taken into account the excluded volume effect between a denaturation bubble and the remained part of the whole polymer chain. They found that this excluded volume effect makes the scaling exponent $\gamma$ in Eq. (4.8) to exceed 2.0.

## 4.2 Secondary structure formation in RNA

In biological bodies RNA usually exists as a single-stranded biopolymer. Similar as DNA, it is also formed by four types of nucleotide bases, G, C, A, and U (Uracil). Two types of canonical Watson-Crick base-pairs, A-U and G-C, can be formed. The non-Watson-Crick base-pairing pattern G-U is also

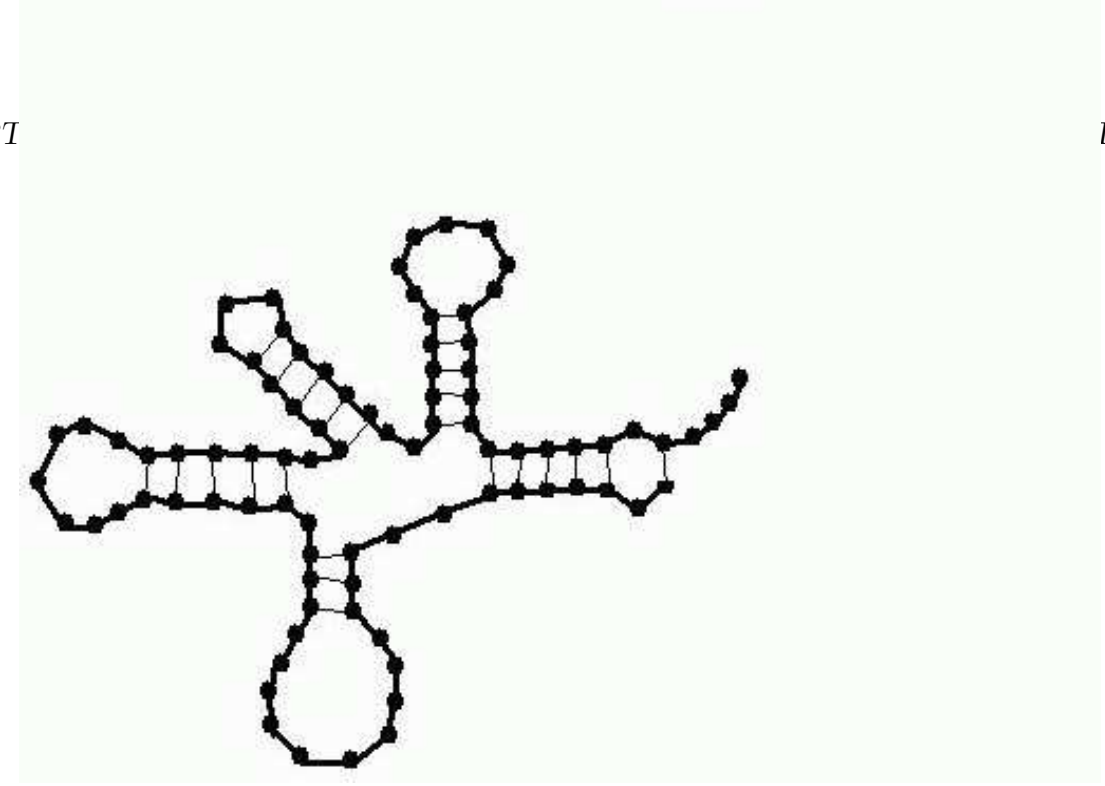

Figure 4.3: A schematic representation of a RNA secondary structure.

quite common in RNA structures. Here we investigate the stability of RNA secondary structures. By the secondary structure we mean the following picture: The position of each nucleotide base along RNA chain with respect to the $5'$-end of RNA is specified by an integer index $i$. Suppose in a RNA secondary structure, nucleotide base at position $i$ and position $j$ (with $j > i$) form a base-pair denoted as pair $(i, j)$, and nucleotide base at position $k$ and position $l$ ($l > k$) forms another base-pair $(k, l)$. Then it is required that base-pairs $(i, j)$ and $(k, l)$ are either *independent*, with $j < k$, or *nested*, with $i < k < l < j$ (see Fig. 4.3). In an actual RNA configuration, some base-pairs may violate these conditions. These base-pairs are classified into the higher-order tertiary structure of RNA. For RNA the main contribution to the free energy is from its secondary structures. Energy contributions from RNA tertiary structures could be regarded as perturbations to the free energy of the system. This separation of energy scales makes the study of RNA secondary structure of particular interest.

When a RNA folds back onto itself and nucleotide bases form base-pairs, many double-helical segments appear. For a RNA made of random sequences, because the correlation along the RNA chain is very weak, each such double-

helical segment in general is very short (of several base-pairs). Such short double-helica segments are very easy to be destroyed. Therefore, secondary structures of a random-sequence RNA are transient, with typical life-time of the order of microseconds. The polymer could easily fluctuate from one secondary structure to another when the environmental temperature is not too low. Entropy plays an important role here.

When one end of the RNA is fixed and the other end is pulled with an external force, it may be energetically unfavorable for the polymer to fold back and form double-helical segments. At some critical force, there is a so-called globule–coil structural transition, where the polymer is stretched considerably straight. As a first step to understand the elastic property of a random-sequence RNA, one can average over the sequence randomness and regard RNA as an effective chain with homogeneous sequence [22]. The RNA chain is modeled as $n+1$ beads connected sequentially by $n$ rigid rods of fixed length $b$. Denote the end-to-end distance vector of such a rigid rod as $\mathbf{r}$, then the distribution of $\mathbf{r}$ is

$$\mu(\mathbf{r}) = \frac{1}{4\pi b^2}\delta(|\mathbf{r}| - b) \ . \tag{4.11}$$

In the absence of external force, the partition function of a RNA segment $(1, n)$ is denoted as $Z_0(1, n; \mathbf{r})$, where $\mathbf{r}$ is the end-to-end distance vector of the RNA segment. When only secondary structures are considered, one can write down the following recursive equation for $Z_0(1, n; \mathbf{r}$:

$$\begin{aligned} Z_0(1,n;\mathbf{r}) &= \int \mathrm{d}\mathbf{r}_1 \mathrm{d}\mathbf{r}_2 \mathrm{Z}_0(1, \mathrm{n}-1; \mathbf{r}_1)\mu(\mathbf{r}_2)\delta(\mathbf{r}-\mathbf{r}_1-\mathbf{r}_2) \\ &+ \Theta(a-|\mathbf{r}|)(e^{\beta\epsilon_\mathrm{b}}-1)\prod_{i=1}^{3}\int \mathrm{d}\mathbf{r}_\mathrm{i}\mu(\mathbf{r}_1)\mathrm{Z}_0(2,\mathrm{n}-1;\mathbf{r}_2)\mu(\mathbf{r}_3)\delta(\mathbf{r}-\sum_{\mathrm{i}=1}^{3}\mathbf{r}_\mathrm{i}) \\ &+ \sum_{m=2}^{n-2}\int\prod_{i=1}^{4}\mathrm{d}\mathbf{r}_\mathrm{i}\Theta(\mathrm{a}-|\mathbf{r}_2+\mathbf{r}_3+\mathbf{r}_4|)(\mathrm{e}^{\beta\epsilon_\mathrm{b}}-1) \\ &\times Z_0(1,m-1;\mathbf{r}_1)\mu(\mathbf{r}_2)Z_0(m+1,n-1;\mathbf{r}_3)\mu(\mathbf{r}_4)\delta(\mathbf{r}-\sum_{i=1}^{4}\mathbf{r}_i) \ , \end{aligned} \tag{4.12}$$

where $\Theta(x)$ is the Heaviside step function; $\epsilon_\mathrm{b}$ is the base-pairing energy.

In the homogeneous chain approximation, the partition function $Z_0(i, j; \mathbf{r})$ depends only on the length $j - i + 1$ of the RNA chain, i.e., $Z_0(i, j; \mathbf{r}) \equiv Z_0(j-i+1; \mathbf{r})$. The boundary condition is $Z_0(1; \mathbf{r}) \equiv \mu(\mathbf{r})$. Under the action

of an external force $\mathbf{f}$, the partition function of a RNA chain with $n$ bonds is

$$Z(n;\mathbf{f}) = \int \mathrm{d}\mathbf{r}\mathrm{Z_0(n;r)e}^{\beta\mathbf{f}\cdot\mathbf{r}} \ . \tag{4.13}$$

Based on Eq. (4.12), one can write down the following recursive equations for $Z(n;\mathbf{r})$:

$$\begin{aligned}
Z(1;\mathbf{f}) &= \tilde{\mu}(\mathbf{f}) \ , && (4.14)\\
Z(2;\mathbf{f}) &= Z(1;\mathbf{f})\tilde{\mu}(\mathbf{f}) \ , && (4.15)\\
Z(3;\mathbf{f}) &= Z(2;\mathbf{f})\tilde{\mu}(\mathbf{f}) + \frac{e^{\beta\epsilon_\mathrm{b}}-1}{(2\pi)^3}\int \mathrm{d}\mathbf{p}\mathrm{v}(\mathbf{f},\mathbf{p})\tilde{\mu}^2(-\mathrm{i}\mathbf{p}/\beta)\mathrm{Z}(1;-\mathrm{i}\mathbf{p}/\beta) \ , && (4.16)\\
Z(n;\mathbf{f}) &= Z(n-1;\mathbf{f})\tilde{\mu}(\mathbf{f}) + \frac{e^{\beta\epsilon_\mathrm{b}}-1}{(2\pi)^3}\int \mathrm{d}\mathbf{p}\mathrm{v}(\mathbf{f},\mathbf{p})\tilde{\mu}^2(-\mathrm{i}\mathbf{p}/\beta)\mathrm{Z(n-2;-i}\mathbf{p}/\beta) \\
&\quad + \sum_{m=1}^{n-3} Z(m;\mathbf{f})\frac{e^{\beta\epsilon_\mathrm{b}}-1}{(2\pi)^3}\int \mathrm{d}\mathbf{p}\mathrm{v}(\mathbf{f},\mathbf{p})\tilde{\mu}^2(-\mathrm{i}\mathbf{p}/\beta)\mathrm{Z(n-m-2;-i}\mathbf{p}/\beta) \ , && (4.17)
\end{aligned}$$

where

$$\tilde{\mu}(\mathbf{f}) \equiv \int \mathrm{d}\mathbf{r}\mu(\mathbf{r})\mathrm{e}^{\beta\mathbf{f}\cdot\mathbf{r}} = \frac{\sinh\beta\mathrm{bf}}{\beta\mathrm{bf}} \ , \tag{4.18}$$

and

$$v(\mathbf{f},\mathbf{p}) = \int \mathrm{d}\mathbf{r}\Theta(\mathrm{a}-|\mathbf{r}|)\mathrm{e}^{\beta\mathbf{f}\cdot\mathbf{r}+\mathrm{i}\mathbf{p}\cdot\mathbf{r}} \ . \tag{4.19}$$

The generation function of the partition function $Z(n;\mathbf{f})$ is then

$$\begin{aligned}
G(z;\mathbf{f}) &\equiv \sum_{n=1}^{\infty} z^n Z(n;\mathbf{f}) && (4.20)\\
&= \Big(1+G(z;\mathbf{f})\Big)\Big(z\tilde{\mu}(\mathbf{f}) + z^2\frac{e^{\beta\epsilon_\mathrm{b}}-1}{(2\pi)^3}\int \mathrm{d}\mathbf{p}\mathrm{v}(\mathbf{f},\mathbf{p})\tilde{\mu}^2(-\mathrm{i}\frac{\mathbf{p}}{\beta})\mathrm{G(z;-i}\frac{\mathbf{p}}{\beta})\Big) && (4.21)
\end{aligned}$$

From Eq. (4.21) one can write down the following equation for $G(z;\mathbf{f})$:

$$G(z;\mathbf{f}) = \frac{z\tilde{\mu}(\mathbf{f})\omega(z;\mathbf{f})}{1-z\tilde{\mu}(\mathbf{f})\omega(z;\mathbf{f})} \ , \tag{4.22}$$

where

$$\omega(z;\mathbf{f}) = 1 + \frac{z}{\tilde{\mu}(\mathbf{f})}\frac{e^{\beta\epsilon_\mathbf{b}}-1}{(2\pi)^3}\int \mathrm{d}\mathbf{p}\mathrm{v}(\mathbf{f},\mathbf{p})\tilde{\mu}^2(-\mathrm{i}\frac{\mathbf{p}}{\beta})\mathrm{G(z;-i}\frac{\mathbf{p}}{\beta}) \ . \tag{4.23}$$

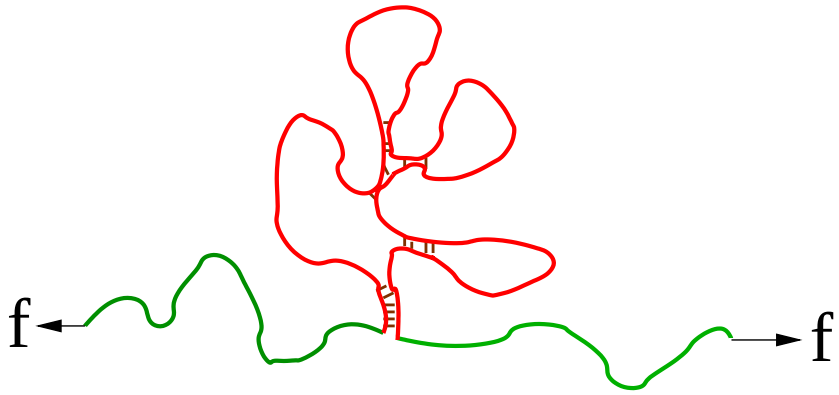


Figure 4.4: Stretching RNA by an external force. A given configuration of a RNA chain can be divided into three parts: two stretched coil segments at both ends, and a complicated globular domain in the middle.

According to the discussion in the previous subsection, we know that the free energy density of the system corresponds to the smallest positive singular point of the generation function $G(z;\mathbf{f})$. At given temperature $T$, when the external force is less than some threshold value $f_c(T)$, the polymer is in a globular phase, with the configuration of RNA fluctuating frequently between many transient secondary structures. The average extension of the polymer is zero. When the force is larger than $f_c(T)$, the polymer is in the stretched coil phase, with few base-pairing interactions. A careful analysis based on Eq. (4.22) and Eq. (4.23) has lead to the conclusion that the force-induced globule–coil transition of RNA is a second-order phase transition process [22]. One can also calculate the elongation of the RNA polymer along the force direction. Here we did not repeat such an analysis but tries to understand the reason for the second-order phase transition from an alternative approach.

The RNA configuration could be divided into three parts: two stretched coil segments at the ends and a (complicated) globular segment in the middle (see Fig. 4.4). The partition function of a coil segment of $n_{\rm c}$ bonds has a very simple scaling form of $Z_{\rm c}(n,f) \sim e^{-n_c\beta g_{\rm c}(f)}$, where $g_{\rm c}(f)$ is the free energy density of a stretched coil segment under the action of an external force $f$. The partition function $Z_{\rm g}(n_{\rm g})$ of a globular segment has the following scaling form:

$$Z_{\rm g}(n_{\rm g}) \sim n_{\rm g}^{-\frac{3}{2}} e^{-n_{\rm g}\beta g_{\rm g}} \ , \tag{4.24}$$

where $g_{\rm g}$ is the free energy density of the RNA chain in the globular state. Most importantly, we notice the scaling exponent $\gamma = 3/2$ in Eq. (4.24). Since this scaling exponent is in the range of $1 < \gamma < 2$, we know from the Lifson argument [18] that the globule–coil transition must be a second-order phase transition. The scaling exponent $\gamma = 3/2$ is caused by the formation of loops in the RNA globular structure [23]. We now give an analytical deduction of Eq. (4.24).

Assume each base of a RNA chain can take only two possible states: in the coil state or form a base-pair with another monomer. In the absence of external force, the partition function of a RNA chain with $n$ bonds can be expressed by the following recursive equation

$$Z_{\rm g}(n) = Z_{\rm g} + e^{\beta\epsilon_{\rm b}} Z_{\rm g}(n-2) + \sum_{l=1}^{n-3} Z_{\rm g}(l) e^{\beta\epsilon_{\rm b}} Z_{\rm g}(n-l-2) \ , \tag{4.25}$$

with $Z_{\rm g}(0) \equiv 1$. The generation function of $Z_{\rm g}(n)$ is

$$G_{\rm g}(z) = \sum_{n=1}^{+\infty} Z_{\rm g}(n) z^n \ . \tag{4.26}$$

Combining Eq. (4.25) and Eq. (4.26) leads to the following expression

$$G_{\rm g}(z) = \frac{1}{2qz^2}(1 - z - 2qz^2 - \sqrt{(1-z)^2 - 4qz^2}) \ , \tag{4.27}$$

where $q = e^{\beta\epsilon_{\rm b}}$. The scaling form of the partition function ($n \gg 1$) could then be obtained:

$$\begin{aligned} Z_{\rm g}(n) &= \frac{1}{2\pi i} \oint \frac{G_{\rm g}(z)}{z^{n+1}} {\rm dz} \\ &= -\frac{1}{4\pi q i} \oint \frac{\sqrt{[1-(1+2\sqrt{q})z][1+(2\sqrt{q}-1)z]}}{z^{n+3}} {\rm dz} \\ &= -\frac{(1+2\sqrt{q})^{n+2}}{4\pi q i} \oint \frac{\sqrt{[1-\zeta][1+\kappa\zeta]}}{\zeta^{n+3}} {\rm d}\zeta \\ &= {\rm const} \times \frac{(1+2\sqrt{q})^n}{n^{3/2}}, \end{aligned} \tag{4.28}$$

where $\kappa = \frac{2\sqrt{q}-1}{2\sqrt{q}+1}$. Therefore, the scaling form Eq. (4.24) is valid.

## 4.3 Collapse transition of surface–confined polymers

To be added in later versions of these notes.

# Chapter 5

# A Brief Introduction to Spin Glasses

In the 1960s it was observed that, at sufficiently low temperatures, some diluted spin systems (Fig. 5.1, middle panel) will be in one of many frozen disordered states.

The average magnetization of such a system is found to be zero, that is

$$m = \frac{1}{N}\sum_{i=1}^{N} m_i = \frac{1}{N}\sum_{i=1}^{N}\langle\sigma_i\rangle = 0 \ , \tag{5.1}$$

where

$$m_i \equiv \langle\sigma_i\rangle \tag{5.2}$$

is the mean magnetization of vertex $i$. Since $m = 0$, the system as a whole has no spontaneous magnetization. This is markedly different from what is expected for an ordinary spin system (see the left panel of Fig. 5.1). However, at low temperatures, the system is not in a paramagnetic phase. The magnetic susceptibility of the system shows a cusp as shown in Fig. 5.1 (right panel). According to the linear response theorem as discussed in Sec. 1.9, the magnetic susceptibility is related to the spin value fluctuations by

$$\chi_i \equiv \frac{\partial m_i}{\partial h_i}\Big|_{h_i=0} = \frac{\langle\sigma_i^2\rangle - \langle\sigma_i\rangle^2}{k_{\rm B}T} = \frac{1 - m_i^2}{k_{\rm B}T} \tag{5.3}$$

If the system were in a paramagnetic phase, then $\chi_i$ should scales as $\chi_i \sim T^{-1}$. The cusp in the magnetic susceptibility indicating that something very interesting was happening.

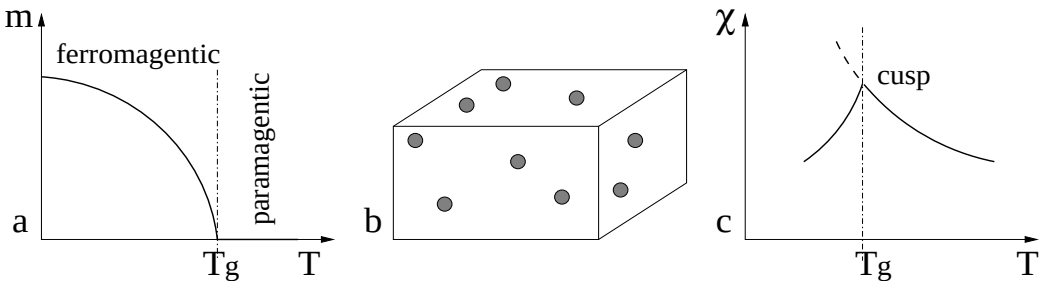


Figure 5.1: (Left) phase diagram of a ferromagnetic system. (Middle) schematic viewing of a randomly diluted spin system. (Right) magnetic susceptibility of a randomly diluted spin system.

The cusp in the magnetic susceptibility can be understood if one assumes that

$$\begin{aligned} m_i &= 0 \qquad \text{for } T \geq T_{\rm g} \ , \\ &\neq 0 \qquad \text{for } T < T_{\rm g} \ , \end{aligned} \tag{5.4}$$

where $T_{\rm g}$ is certain characteristic temperature (the spin glass transition temperature). In other words, at low temperatures, the spins of the system may be partially frozen to a disordered pattern with no net whole magnetization.

Theoretical investigations on spin glasses began with the article of Edwards and Anderson in 1975. Early efforts on this branch of statistical physics were reviewed in [24, 25, 26]. In this part of this chapter, we only briefly mention some basic concepts and inherent difficulties of this field.

## 5.1 Disorder and frustration

Consider the following model Hamiltonian due to Edwards and Anderson

$$H = -\sum_{(i,j)} J_{ij}\sigma_i\sigma_j \ , \tag{5.5}$$

where the spin spin coupling $J_{ij}$ is not a constant but is a *quenched* random variable with mean zero (for example, $J_{ij} = \pm J_0$ with equal probability). Given a sample, the couplings $J_{ij}$ are then fixed and can not change with time.

Quenched disorder leads to frustration in a looped system. Frustration means that, it is impossible to satisfy all the "constraints" *simultaneously*. Figure 5.2 gives a very simple example.

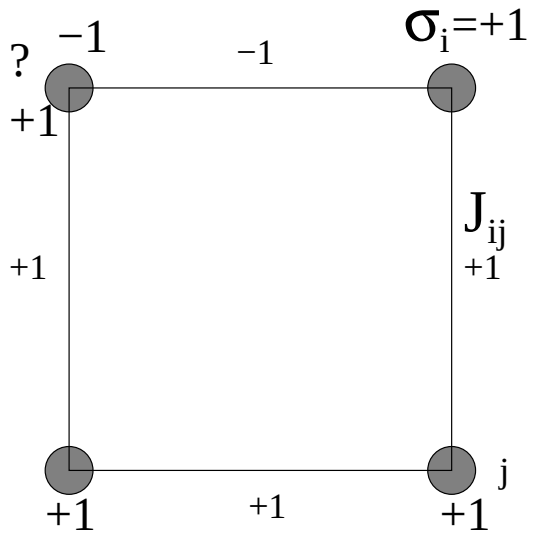


Figure 5.2: Quenched disorder leads to frustration.

## 5.2 Ergodicity breaking and pure states

$$\langle A\rangle = \sum_{\alpha=1}^{n}\sum_{\vec{\sigma}\in\alpha}\frac{A(\vec{\sigma})e^{-\beta H_J(\vec{\sigma})}}{Z} = \sum_{\alpha=1}^{n}\omega_\alpha\langle A\rangle_\alpha \ , \tag{5.6}$$

where

$$\omega_\alpha = \frac{\sum\limits_{\vec{\sigma}\in\alpha} e^{-\beta H_J(\vec{\sigma})}}{Z} \equiv \frac{Z_\alpha}{Z} \tag{5.7}$$

In the case of ergodicity breaking, the definition of the partition function by Eq. (1.16) with the summation over all the microscopic configuration $\mathbf{s}$ of the system has no physical meaning.

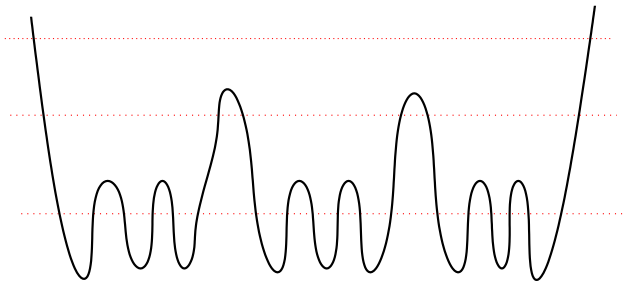

Figure 5.3: Ergodicity breaking and proliferation of pure states.

## 5.3 Self-averaging

At given set of quenched coupling constants $J_{ij}$, the free energy is

$$F_J = -k_B T \log \sum_{\{\vec{s}\}} e^{-\beta H_J(\vec{s})} \ , \tag{5.8}$$

and the entropy is

$$S_J = -k_B \sum_{\vec{s}} \rho_J(\vec{s}) \log \rho_J(\vec{s}) \ . \tag{5.9}$$

The self-averaging property means that, for a typical realization of the couplings $J_{ij}$,

$$F_J = \overline{F} \equiv [F_J]_J \ , \tag{5.10}$$

$$S_J = \overline{S} \equiv [S_J]_J \ , \tag{5.11}$$

where

$$[A_J]_J \equiv \int \mathcal{D}J \mathrm{Prob}(J) A_J \ . \tag{5.12}$$

To calculate the average over the logarithm in Eq. (5.8), one may use the replica trick:

$$[\ln Z_J]_J = \lim_{n\to 0} \frac{\ln\Big([Z_J^n]_J\Big)}{n} \ , \tag{5.13}$$

and

$$\begin{aligned} [A_J]_J &= \Big[\frac{\sum_\sigma A_J(\sigma) e^{-\beta H_J(\sigma)}}{Z_J}\Big]_J \\ &= \lim_{n\to 0} \int \mathrm{d}\sigma_1 \ldots \int \mathrm{d}\sigma_\mathrm{n} \Big[\mathrm{A_J}(\sigma_1) \exp(-\beta \mathrm{H_J}(\sigma_1) - \ldots - \beta \mathrm{H_J}(\sigma_\mathrm{n}))\Big]_\mathrm{J} \ . \end{aligned} \tag{5.14}$$

# Chapter 6

# The $p$-Spin Spherical Model and the Replica Method

The infinite-connectivity $p$-spin spherical model (reviewed in [27]) is defined as follows:

$$H_J = -\sum_{i_1<\ldots<i_p} J_{i_1\ldots i_p}\sigma_{i_1}\sigma_{i_2}\ldots\sigma_{i_p} \ , \tag{6.1}$$

where the 'spin' state variable $\sigma_i$ is real-valued in the range $-\infty < \sigma_i < +\infty$. There is the following constraint that

$$\sum_{i=1}^{N}\sigma_i^2 = N \ . \tag{6.2}$$

In Eq. (6.1), the coupling constants $J_{i_1\ldots i_p}$ are quenched random variables. They are independently and identically distributed according to

$$\text{Prob}(J_{i_1\ldots i_p}) \propto \exp\!\left(-\frac{J_{i_1\cdots i_p}}{p!J_0^2/N^{p-1}}\right) \ . \tag{6.3}$$

We are interested in obtaining the mean free energy of the system $\overline{F}$ as defined in Eq. (5.10) as a function of temperature $T$.

## 6.1 The annealed approximation

$$\overline{F} \equiv \left[\ln Z_J\right]_J \ . \tag{6.4}$$

The annealed approximation consists in replacing $\left[\ln Z_J\right]_J$ with $\ln[Z_J]_J$.

$$\begin{aligned}
\overline{Z} &\equiv [Z_J]_J \\
&= \int \mathcal{D}J \mathrm{Prob}(J) \sum_{\sigma} \exp(\beta \sum\nolimits' J_{i_1 \ldots i_p} \sigma_{i_1} \ldots \sigma_{i_p}) \qquad (6.5) \\
&= \int\limits_{|\sigma|=\sqrt{N}} \mathrm{d}\sigma \exp\Big( \frac{(\beta \mathrm{J}_0)^2}{4\mathrm{N}^{\mathrm{p}-1}} (\sum_{\mathrm{i}=1}^{\mathrm{N}} \sigma_{\mathrm{i}}^2)^{\mathrm{p}} \Big) \\
&= \exp(N \frac{\beta^2 J_0^2}{4} S_N(N^{1/2}) \ , \qquad (6.6)
\end{aligned}$$

where

$$S_N(N^{1/2}) = \frac{2\pi^{N/2} N^{(N-1)/2}}{\Gamma(N/2)} \qquad (6.7)$$

is the surface area of a $N$-dimensional sphere of radius $N^{1/2}$.

The free energy as estimated by the annealed approximation is then

$$\begin{aligned}
\overline{F}_{\mathrm{anneal}} &= -k_B T \ln \overline{Z} \qquad (6.8) \\
&= N[-\frac{J_0^2}{k_{\mathrm{B}} T} - T s_\infty] \ , \qquad (6.9)
\end{aligned}$$

where

$$s_\infty = k_{\mathrm{B}} \frac{\ln S_N(N^{1/2})}{N} = k_{\mathrm{B}} \ln 2\pi e \ . \qquad (6.10)$$

At high temperatures, disorder is irrelevant. The annealed free energy density is actually identical to the free energy density of this model system. At low temperatures, however, quenched disorder becomes relevant. In the later case, the annealed free energy density gives only a *lower* bound to the true free energy density.

## 6.2 The replica method

Now use the replica trick to calculate the free energy density of the system.

$$\overline{\ln Z} = \lim_{n \to 0} \frac{\ln \overline{Z^n}}{n} \ . \qquad (6.11)$$

To perform the limit of $n \to 0$, we first obtain the expression for $\overline{Z^n}$ for each integer $n$; then we assume that this expression can be analytically extended to non-integer $n$ values!

Since

$$Z_J^n = \int \mathrm{d}\vec{\sigma}^1 \cdots \int \mathrm{d}\vec{\sigma}^{\mathrm{n}} \mathrm{e}^{-\beta \sum\limits_{\alpha=1}^{\mathrm{n}} \mathrm{H_J}(\vec{\sigma}^\alpha)} , \tag{6.12}$$

its average over the quenched disorder is

$$\begin{aligned}
\overline{Z^n} &= \sum_{\{\vec{\sigma}^1, \vec{\sigma}^2 \cdots \vec{\sigma}^n\}} \prod_{i_1 < i_2 < \cdots < i_p} \exp\Big[ \frac{p!(\beta J_0)^2}{4N^{p-1}} (\sum_{\alpha=1}^{n} \sigma_{i_1}^\alpha \sigma_{i_2}^\alpha \cdots \sigma_{i_p}^\alpha)^2 \Big] \\
&= \sum_{\{\vec{\sigma}^1, \vec{\sigma}^2 \cdots \vec{\sigma}^n\}} \exp\Big[ N \frac{(\beta J_0)^2}{4} \sum_{\alpha=1}^{n} \sum_{\beta=1}^{n} (\frac{\sum\limits_{j=1}^{N} \sigma_j^\alpha \sigma_j^\beta}{N})^p \Big] \\
&\equiv \sum_{\{\vec{\sigma}^1, \vec{\sigma}^2 \cdots \vec{\sigma}^n\}} \prod_{\alpha=1}^{n} \delta(Q_{\alpha\alpha} - \frac{1}{N} \sum_{i=1}^{N} \sigma_i^\alpha \sigma_j^\alpha) \times \\
&\quad \prod_{\alpha<\beta} \int \mathrm{dQ}_{\alpha\beta} \delta(\mathrm{Q}_{\alpha\beta} - \frac{1}{\mathrm{N}} \sum_{\mathrm{i}=1}^{\mathrm{N}} \sigma_{\mathrm{i}}^\alpha \sigma_{\mathrm{j}}^\beta) \times \\
&\quad \exp\Big[ N \frac{(\beta J_0)^2}{2} (\frac{1}{2} \sum_{\alpha=1}^{n} Q_{\alpha\alpha}^p + \sum_{\alpha<\beta} Q_{\alpha\beta}^p) \Big] .
\end{aligned} \tag{6.13}$$

We can use the Fourier expansion of Dirac's delta function

$$\delta(x) \equiv \int_{-\infty}^{\infty} \mathrm{d}\lambda \mathrm{e}^{\mathrm{i}\lambda \mathrm{x}} \tag{6.14}$$

and re-write Eq. (6.14) into another form

$$\begin{aligned}
\overline{Z^n} &= \int \prod_{\alpha<\beta} \int \mathrm{d}\lambda_{\alpha\beta} \prod_{\alpha} \int \mathrm{d}\lambda_{\alpha\alpha} \prod_{\alpha<\beta} \int \mathrm{dQ}_{\alpha\beta} \prod_{\mathrm{j}=1}^{\mathrm{N}} \int \mathrm{d}\sigma_{\mathrm{j}}^1 \cdots \int \mathrm{d}\sigma_{\mathrm{j}}^{\mathrm{n}} \times \\
&\quad \exp\Big[ N \frac{(\beta J_0)^2}{4} \sum_{\alpha\beta} Q_{\alpha\beta}^p + N \sum_{\alpha\beta} i\lambda_{\alpha\beta} Q_{\alpha\beta} - i \sum_{i=1}^{N} \lambda_{\alpha\beta} \sigma_i^\alpha \sigma_i^\beta \Big] \\
&= \int \prod_{\alpha<\beta} \int \mathrm{d}\lambda_{\alpha\beta} \prod_{\alpha} \int \mathrm{d}\lambda_{\alpha\alpha} \prod_{\alpha<\beta} \int \mathrm{dQ}_{\alpha\beta} \exp\Big( -\mathrm{NS}(\mathrm{Q}, \lambda) \Big) ,
\end{aligned} \tag{6.15}$$

where

$$S(Q, \lambda) = -\frac{(\beta J_0)^2}{4} \sum_{\alpha\beta} Q_{\alpha\beta}^p - \sum_{\alpha\beta} i\lambda_{\alpha\beta} Q_{\alpha\beta} + \frac{1}{2} \ln \mathrm{Det}(i\lambda_{\alpha\beta}) . \tag{6.16}$$

The free energy density is then

$$\begin{aligned} -\beta f &= -\lim_{N\to\infty}\lim_{n\to 0}\frac{\ln\overline{Z^n}}{Nn} \\ &= \frac{1}{2}\ln\pi + \lim_{N\to\infty}\lim_{n\to 0}\frac{1}{Nn}\ln\Big[\int \mathcal{D}\lambda_{\alpha\beta}\int \mathcal{D}Q_{\alpha\beta}e^{-NS(Q,\lambda)}\Big] \ . \end{aligned} \tag{6.17}$$

The maximal point at fixed $Q$ values is determined by

$$\frac{\partial S(Q,\lambda)}{\partial \lambda_{\alpha\beta}} = 0 \quad \Longrightarrow \quad 2i\lambda_{\alpha\beta} = [Q^{-1}]_{\alpha\beta} \ . \tag{6.18}$$

Inserting Eq. (6.18) into Eq. (6.17) we finally obtain that

$$f = -Ts_\infty - k_{\rm B}T\lim_{n\to 0}\frac{\frac{(\beta J_0)^2}{4}\sum\limits_{\alpha\beta}Q^p_{\alpha\beta} + \frac{1}{2}\ln {\rm Det}Q}{n} \ , \tag{6.19}$$

where the elements of the matrix $Q$ satisfies

$$\frac{p(\beta J_0)^2}{2}Q^{p-1}_{\alpha\beta} + \left(Q^{-1}\right)_{\alpha\beta} = 0 \ . \tag{6.20}$$

## 6.3 The replica symmetric solution

As a first attempt to solve Eq. (6.20), let us assume the following form for the overlap matrix $Q$:

$$Q = \begin{bmatrix} 1 & q_0 & q_0 & \cdots & q_0 \\ q_0 & 1 & q_0 & \cdots & q_0 \\ q_0 & q_0 & 1 & \cdots & q_0 \\ \cdots & \cdots & \cdots & \cdots & \cdots \\ q_0 & q_0 & \cdots & q_0 & 1 \end{bmatrix} \tag{6.21}$$

Then it is easy to verify that the inverse matrix of $Q$ is

$$\left(Q^{-1}\right)_{\alpha\beta} = \frac{1}{1-q_0}\delta^\beta_\alpha - \frac{q_0}{(1-q_0)(1+(n-1)q_0)} \ . \tag{6.22}$$

In the limit of $n \to 0$, Eq. (6.20) reduces to

$$\frac{1}{2}(\beta J_0)^2 p q_0^{p-1} - \frac{q_0}{(1-q_0)^2} = 0 \ . \tag{6.23}$$

The free energy density Eq. (6.19) for this replica-symmetric solution is

$$f = -Ts_\infty - k_{\rm B}T\frac{(\beta J_0)^2}{4} + k_{\rm B}T\left(\frac{(\beta J_0)^2}{4}q_0^p - \frac{\ln(1-q_0)}{2} - \frac{q_0(1-q_0)}{2}\right) . \quad (6.24)$$

For the special case of $p = 2$ (two-body interaction), Eq. (6.23) predicts a continuous spin glass phase transition with

$$\begin{aligned} q_0 &= 0 \qquad\qquad T > T_{\rm sg}^{(2)} , \quad (6.25)\\ &= 1 - \frac{T}{T_{\rm sg}^{(2)}} \qquad T \le T_{\rm sg}^{(2)} , \end{aligned}$$

where the spin glass transition temperature $T_{\rm sg}^{(2)} = J_0/k_{\rm B}$.

For the general case of $p > 2$, the spin glass phase transition is discontinuous. As an example, let us consider the case of $p = 4$. In this case, Eq. (6.23) predicts that

$$\begin{aligned} q_0 &= 0 \qquad\qquad T > T_{\rm sg}^{(4)} , \quad (6.26)\\ &= 1/2 + \sqrt{1 - T/T_{\rm sg}^{(4)}}/2 \qquad T \le T_{\rm sg}^{(4)} , \end{aligned}$$

where $T_{\rm sg}^{(4)} = 2^{-3/2}J_0/k_{\rm B}$.

Below the spin glass transition temperature, the replica-symmetric solution of the p-spin spherical model is found to be unstable [28, 29]. The physical picture behind this replica-symmetric solution is wrong. To see this, in the next section we will discuss more about the physical meaning of the overlap matrix $Q$.

## 6.4 Relation between replica symmetry breaking and ergodicity breaking

$$\begin{aligned} q^{(1)} &\equiv \frac{1}{N}\sum_{i=1}^{N}\overline{\langle\sigma_i\rangle^2} = \frac{1}{N}\sum_{i=1}^{N}\overline{[\sum_\alpha \omega_\alpha\langle\sigma_i\rangle_\alpha]^2} \quad (6.27)\\ &= \frac{1}{N}\sum_{i=1}^{N}\overline{\sum_\alpha\sum_\beta \omega_\alpha\omega_\beta\langle\sigma_j\rangle_\alpha\langle\sigma_j\rangle_\beta} \quad (6.28)\\ &= \overline{\sum_{\alpha\beta}\omega_\alpha\omega_\beta q_{\alpha\beta}} \quad (6.29) \end{aligned}$$

$$= \int \mathrm{dq}\overline{\sum_{\alpha\beta}\omega_\alpha\omega_\beta\delta(\mathrm{q}-\mathrm{q}_{\alpha\beta})}\mathrm{q} \tag{6.30}$$

$$= \int \mathrm{dq}\overline{\mathrm{P(q)}}\mathrm{q}\ . \tag{6.31}$$

In the above listed equations, the overline indicates averaging over all the realizations of the quenched disorder. The parameter $\omega_\alpha$ means the statistical weight of pure state $\alpha$ [see Eq. (5.7)];

$$q_{\alpha\beta} = \frac{1}{N}\sum_{i=1}^{N}\langle\sigma_j\rangle_\alpha\langle\sigma_j\rangle_\beta \tag{6.32}$$

is the overlap between two pure states in a given realization of the quenched disorder; and

$$\overline{P(q)} = \overline{\sum_{\alpha\beta}\omega_\alpha\omega_\beta\delta(q-q_{\alpha\beta})} \tag{6.33}$$

is the overlap distribution of $q_{\alpha\beta}$ averaged over all the realizations of quenched disorder.

Similarly, for higher order moments, we find that

$$q^{(k)} \equiv \frac{1}{N^k}\sum_{i_1=1}^{N}\cdots\sum_{i_k=1}^{N}\overline{\langle\sigma_{i_1}\cdots\sigma_{i_k}\rangle^2} \tag{6.34}$$

$$= \frac{1}{N^k}\sum_{i_1\cdots i_k}\overline{\sum_\alpha\sum_\beta\omega_\alpha\omega_\beta\langle\sigma_{i_1}\ldots\sigma_{i_k}\rangle_\alpha\langle\sigma_{i_1}\ldots\sigma_{i_k}\rangle_\beta} \tag{6.35}$$

$$= \frac{1}{N^k}\sum_{i_1\cdots i_k}\overline{\sum_\alpha\sum_\beta\omega_\alpha\omega_\beta\langle\sigma_{i_1}\rangle_\alpha\ldots\langle\sigma_{i_k}\rangle_\alpha\langle\sigma_{i_1}\rangle_\beta\ldots\langle\sigma_{i_k}\rangle_\beta} \tag{6.36}$$

$$= \overline{\sum_\alpha\sum_\beta\omega_\alpha\omega_\beta\delta(q-q_{\alpha\beta})q_{\alpha\beta}^k} = \int \mathrm{dq}\overline{\mathrm{P(q)}}\mathrm{q}^{\mathrm{k}}\ . \tag{6.37}$$

In going from Eq. (6.35) to Eq. (6.36) we have used the so-called clustering property of a pure state, i.e.,

$$\langle\sigma_{i_1}\ldots\sigma_{i_k}\rangle_\alpha = \langle\sigma_{i_1}\rangle_\alpha\ldots\langle\sigma_{i_k}\rangle_\alpha \tag{6.38}$$

for a set of randomly chosen vertices $\{i_1,\ldots,i_k\}$ [25, 27].

Equations (6.31) and (6.37) means that, the overlap distribution $\overline{P(q)}$ can be obtained if we know the value of $q^{(k)}$ for each $k = 1, 2, \ldots, \infty$. On the

hand, the moments $q^{(k)}$ can be calculated through the replica method. For example,

$$q^{(1)} = \frac{1}{N}\sum_{i=1}^{N}\overline{\frac{1}{Z^2}\int \mathrm{d}\vec{\sigma}^1\sigma_{\mathrm{i}}^1 \mathrm{e}^{-\beta \mathrm{H_J}(\vec{\sigma}^1)}\int \mathrm{d}\vec{\sigma}^2\sigma_{\mathrm{i}}^2 \mathrm{e}^{-\beta \mathrm{H_J}(\vec{\sigma}^2)}} \tag{6.39}$$

$$= \lim_{n\to 0}\frac{1}{N}\sum_{i=1}^{N}\overline{\int \mathrm{d}\vec{\sigma}^1 \ldots \int \mathrm{d}\vec{\sigma}^{\mathrm{n}}\sigma_{\mathrm{i}}^1\sigma_{\mathrm{i}}^2 \exp(-\beta\sum_{\alpha=1}^{\mathrm{n}}\mathrm{H_J}(\vec{\sigma}^\alpha))} \tag{6.40}$$

$$= \int \mathcal{D}Q_{\alpha\beta} e^{-NS\left(Q,\lambda(Q)\right)} = Q_{12} = \lim_{n\to 0}\frac{2}{n(n-1)}\sum_{\alpha>\beta}Q_{\alpha\beta}\ . \tag{6.41}$$

In Eq. (6.41), $Q_{\alpha\beta}$ is the fixed point solution of Eq. (6.20). The higher order moments can also be expressed in terms of the order parameters $Q$. The explicit expression is

$$q^{(k)} = Q_{12}^k = \lim_{n\to 0}\frac{2}{n(n-1)}\sum_{\alpha>\beta}Q_{\alpha\beta}^k\ . \tag{6.42}$$

Based on Eq. (6.42) and Eq. (6.37), we finally obtain the following expression that

$$\overline{P(q)} = \lim_{n\to 0}\frac{2}{n(n-1)}\sum_{\alpha>\beta}\delta(q-Q_{\alpha\beta})\ . \tag{6.43}$$

**The average probability that two pure states of the system have overlap $q$ is equal to the fracture of non-diagonal elements of the overlap matrix $Q$ equal to $q$.**

The replica-symmetric solution of the previous section has

$$\overline{P(q)} = \delta(q-q_0)\ , \tag{6.44}$$

Since the overlap ditribution $\overline{P(q)}$ also includes the overlap of a pure state with itself. If this distribution is of the form Eq. (6.44), then the underlying picture must be that, the system contains only one single pure state, i.e., ergodicity is not broken. At low temperatures this picuture is in-correct. When ergodicity is broken, $\overline{P(q)}$ must have several peaks, and therefore, the off-diagonal elements of the overlap matrix $Q$ must not all be equal.

## 6.5 First-order replica symmetry breaking solution

As the simplest replica-symmetry-breaking solution, we assume that the off-diagonal elements of matrix $Q$ can take on two different values $q_0$ and $q_1$. And we assume the following form for matrxi $Q$:

$$Q = \begin{bmatrix} 1 & q_1 & \cdots & q_1 & & & & & & & & \\ q_1 & 1 & \cdots & q_1 & & & & & & & & \\ \cdots & \cdots & \cdots & \cdots & & & & & q_0 & & & \\ q_1 & \cdots & q_1 & 1 & & & & & & & & \\ & & & & 1 & q_1 & \cdots & q_1 & & & & \\ & & & & q_1 & 1 & \cdots & q_1 & & & & \\ & & & & \cdots & \cdots & \cdots & \cdots & & & & \\ & & & & q_1 & \cdots & q_1 & 1 & & & & \\ & & & & & & & & \ddots & & & \\ & & & & & & & & & 1 & q_1 & \cdots & q_1 \\ & & & q_0 & & & & & & q_1 & 1 & \cdots & q_1 \\ & & & & & & & & & \cdots & \cdots & \cdots & \cdots \\ & & & & & & & & & q_1 & \cdots & q_1 & 1 \end{bmatrix} \tag{6.45}$$

In each row of matrxi $Q$, there are $m-1$ elements with value $q_1$ and $n-m$ elements with value $q_0$. The physical picture behind Eq. (6.45) is schematically shown in Fig. 6.1.

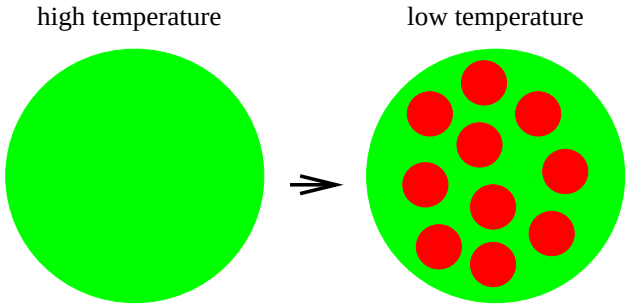


Figure 6.1: First-order replica-symmetry-breaking.

The overlap distribution is then

$$\begin{aligned}\overline{P(q)} &= \lim_{n\to 0}\frac{n(n-m)\delta(q-q_0)+n(m-1)\delta(q-q_1)}{n(n-1)} \\ &= m\delta(q-q_0)+(1-m)\delta(q-q_1)\ . \end{aligned} \tag{6.46}$$

In the limit of $n \to 0$, the parameter $m$ should be interpreted as a probability, with $0 \le m \le 1$.

For this solution, we have

$$\mathrm{Det}(Q) = (1-q_1)^{n-\frac{n}{m}}[1-q_1+m(q_1-q_0)]^{\frac{n}{m}-1}[nq_0+m(q_1-q_0)+1-q_1]\ . \tag{6.47}$$

The free energy density is

$$\begin{aligned} f &= -TS_\infty - \frac{J_0^2}{4k_{\rm B}T} - \frac{J_0^2}{4k_{\rm B}T}(m-1)q_1^p + \frac{J_0^2}{4k_{\rm B}T}mq_0^p \\ &\quad -\frac{1}{2}k_{\rm B}T(1-\frac{1}{m})\ln(1-q_1) - \frac{k_{\rm B}T}{2m}\ln[1-q_1+m(q_1-q_0)] \\ &\quad -\frac{1}{2}k_{\rm B}T\frac{q_0}{1-q_1+m(q_1-q_0)}\ . \end{aligned} \tag{6.48}$$

The order parameters $q_0$, $q_1$, and $m$ can be calculated by requiring the first-order derivative of the free energy density $f$ with respective to these parameters be zero. Then we find that $q_0 = 0$. The other two order parameters are determined by the following coupled equaions

$$\frac{1}{2}(\beta J_0)^2 q_1^p + \frac{1}{m^2}\log\frac{1-q_1}{1-(1-m)q_1} + \frac{1}{m}\frac{q_1}{1-(1-m)q_1} = 0\ , \tag{6.49}$$

$$\frac{1}{2}(\beta J_0)^2 p q_1^{p-2} - \frac{1}{(1-q_1)[1-(1-m)q_1]} = 0\ . \tag{6.50}$$

For $p = 4$, the solution of Eqs. (6.49) and Eq. (6.50) are shown in Fig. 6.2.

For the $p$-spin spherical model, it turns out that the first-order replica-symmetry-breaking solution is stable. Therefore, higher order replica-symmetry-breaking scheme is not needed. This is a special property of the sperical model. In general, full replica-symmetry-breaking is needed to describe the low-temperature behavior of a given spin glass system.

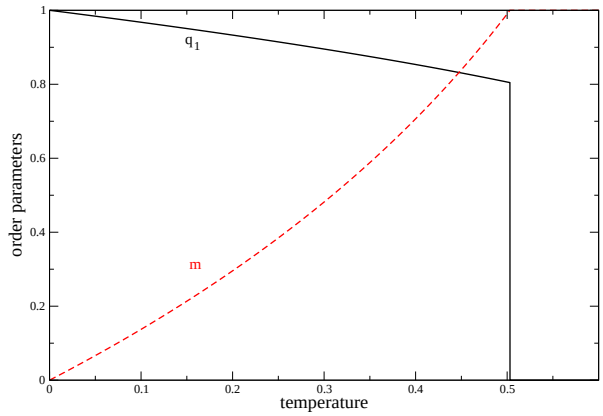


Figure 6.2: The order parameter $q_1$ and $m$ for the $p = 4$-spin spherical model.

# Chapter 7

# The cavity Approach to Finite-Connectivity Spin Glasses

to be added soon.

# Chapter 8

# Spin Glass Physics and Optimization Problems

Examples of non-deterministic polynomial complete (NP-complete) problems [30]:

**3-satisfiability.** A Boolean formula involving $N$ variables and $M$ clauses of length 3:

$$(x_1 \cap x_2 \cap x_3) \cup (\overline{x_1} \cap x_2 \cap \overline{x_3}) \cup (x_1 \cap \overline{x_2} \cap \overline{x_3})$$

**vertex covering.** Covering a graph with at most $m$ markers.

**graph coloring.** Coloring a graph with at most $p$ colors.

Discussions on the application of statistical physics of spin glasses to hard combinatorial optimization problems (see, e.g., [31, 7, 8, 32, 33, 34, 9, 35, 36]) will be added in a later version of these lecture notes.

# Bibliography


[1] Landau, L & Lifshitz, E. M. (1958) *Statistical Physics.* (Pergamon, London).

[2] Kadanoff, L. P. (1999) *Statistical Physics: Statics, Dynamics and Renormalization.* (World Scientific, Singapore).

[3] Ma, S. K. (1976) *Modern Theory of Critical Phenomena.* (Benjamin).

[4] Stanley, H. E. (1987) *Introduction to Phase Transition and Critical Phenomena.* (Oxford Univ. Press, Oxford).

[5] Bethe, H. A. (1935) Statistical theory of superlattices *Proc. R. Soc. London A* **150**, 552–575.

[6] Bollobás, B. (1985) *Random Graphs.* (Academic Press, Landon).

[7] Mézard, M & Parisi, G. (2001) The bethe lattice spin glass revisited *Eur. Phys. J. B* **20**, 217–233.

[8] Mézard, M & Parisi, G. (2003) The cavity method at zero temperature *J. Stat. Phys.* **111**, 1–34.

[9] Zhou, H. (2003) Vertex cover problem studied by cavity method: Analytics and population dynamics *Eur. Phys. J. B* **32**, 265–270.

[10] Kschischang, F. R, Frey, B. J, & Loeliger, H.-A. (2001) Factor graphs and the sum-product algorithm *IEEE Trans. Infor. Theor.* **47**, 498–519.

[11] Montanari, A & Rizzo, T. (2005) How to compute loop corrections to bethe approximation *J. Stat. Mech.: Theo. Exp.* **2005**, P10011.

[12] Parisi, G & Slanina, F. (2006) Loop expansion around the bethe-peierls approximation for lattice models *J. Stat. Mech.: Theo. Exp.* **2006**, L02003.

[13] Saenger, W. (1984) *Principles of Nucleic Acid Structure*. (Springer-Verlag, New York).

[14] Zhou, H, Zhang, Y, & Ou-Yang, Z.-C. (1999) Bending and base-stacking interactions in double-stranded dna *Phys. Rev. Lett.* **82**, 4560–4563.

[15] Essevaz-Roulet, B, Bockelmann, U, & Heslot, F. (1997) Mechanical separation of the complementary strands of dna *Proc. Natl. Acad. Sci. USA* **94**, 11935–11940.

[16] Poland, D & Scheraga, H. A. (1966) Occurrence of a phase transition in nucleic acid models *J. Chem. Phys.* **45**, 1464–1469.

[17] Poland, D & Scheraga, H. A. (1970) *Theory of Helix-Coil Transitions in Biopolymers: Statistical Mechanical Theory of Order-Disorder Transitions in Biological Macromolecules*. (Academic Press, New York).

[18] Lifson, S. (1964) Partition functions of linear-chain molecules *J. Chem. Phys.* **40**, 3705–3710.

[19] Fisher, M. E. (1966) Effect of excluded volume on phase transitions in biopolymers *J. Chem. Phys.* **45**, 1469–1473.

[20] Zhou, H, Zhang, Y, & Ou-Yang, Z.-C. (2005) in *Handbook of Theoretical and Computational Nanotechnology*, eds. Rieth, M & Schommers, W. (American Scientific Publishers, California) Vol. 10, pp. 1–69.

[21] Kafri, Y, Mukamel, D, & Peliti, L. (2000) Why is the dna denaturation transition first order? *Phys. Rev. Lett.* **85**, 4988–4991.

[22] Montanari, A & Mézard, M. (2001) Hairpin formation and elongation of biomolecules *Phys. Rev. Lett.* **86**, 2178–2181.

[23] Bundschuh, R & Hwa, T. (1999) Rna secondary structure formation: A solvable model of heteropolymer folding *Phys. Rev. Lett.* **83**, 1479–1482.

[24] Binder, K & Young, A. P. (1986) Spin glasses: Experimental facts, theoretical concepts, and open questions *Rev. Mod. Phys.* **58**, 801–976.

[25] Mézard, M, Paris, G, & Virasoro, M. A. (1987) *Spin Glass Theory and Beyond*. (World Scientific, Singapore).

[26] Fischer, K. H & Hertz, J. A. (1991) *Spin Glasses*. (Cambridge Univ. Press, Cambridge).

[27] Castellani, T & a. Cavagna. (2005) Spin-glass theory for pedestrians *J. Stat. Mech.: Theo. Exp.* **2005**, P05012.

[28] De Almeida, J. R. L & Thouless, D. J. (1978) Stability of the sherrington-kirkpatrick solution of a spin glass model *J. Phys. A: Math. Gen.* **11**, 983.

[29] Crisanti, A & Sommers, H.-J. (1992) The spherical $p$-spin interaction spin glass model: the statics *Z. Phys. B* **87**, 341–354.

[30] Garey, M & Johnson, D. S. (1979) *Computers and Intractability: A Guide to the Theory of NP-Completeness*. (Freeman, San Francisco).

[31] Dubois, O, Monasson, R, Selman, B, & Zecchina, R, eds. (2001) *Phase Transitions in Combinatorial Problems* Vol. 265, pp. 1–308.

[32] Mézard, M, Parisi, G, & Zecchina, R. (2002) Analytic and algorithmic solution of random satisfiability problems *Science* **297**, 812–815.

[33] Mézard, M & Zecchina, R. (2002) The random k-satisfiability problem: from an analytic solution to an efficient algorithm *Phys. Rev. E* **66**, 056126.

[34] Braunstein, A, Mézard, M, & Zecchina, R. (2005) Survey propagation: An algorithm for satisfiability *Random Struct. Algorith.* **27**, 201–226.

[35] Zhou, H. (2005) Long-range frustration in a spin-glass model of the vertex-cover problem *Phys. Rev. Lett.* **94**, 217203.

[36] Zhou, H. (2005) Long-range frustration in finite connectivity spin glasses: a mean-field theory and its application to the random $k$-satisfiability problem *New J. Phys.* **7**, 123.